NAVAL POSTGRADUATE SCHOOL
Monterey, California

THESIS

SEASONAL VARIABILITY
IN THE CALIFORNIA CURRENT,
A DIECAST MODEL STUDY

by

Joseph R. Donato

December 1998

Thesis Advisor: Robert L. Haney

Approved for public release; distribution is unlimited.

REPORT DOCUMENTATION PAGE		Form Approved OMB No. 0704-0188

Public reporting burden for this collection of information is estimated to average 1 hour per response, including the time for reviewing instruction, searching existing data sources, gathering and maintaining the data needed, and completing and reviewing the collection of information. Send comments regarding this burden estimate or any other aspect of this collection of information, including suggestions for reducing this burden, to Washington Headquarters Services, Directorate for Information Operations and Reports, 1215 Jefferson Davis Highway, Suite 1204, Arlington, VA 22202-4302, and to the Office of Management and Budget, Paperwork Reduction Project (0704-0188) Washington DC 20503.

1. AGENCY USE ONLY (Leave blank)	2. REPORT DATE December 1998	3. REPORT TYPE AND DATES COVERED Master's Thesis
4. TITLE AND SUBTITLE SEASONAL VARIABILITY IN THE CALIFORNIA CURRENT, A DIECAST MODEL STUDY		5. FUNDING NUMBERS
6. AUTHOR(S) Donato, Joseph R		
7. PERFORMING ORGANIZATION NAME(S) AND ADDRESS(ES) Naval Postgraduate School Monterey CA 93943-5000		8. PERFORMING ORGANIZATION REPORT NUMBER
9. SPONSORING/MONITORING AGENCY NAME(S) AND ADDRESS(ES) Office of Naval Research Navy Ocean Modeling and Prediction 800 N. Quincy St. Arlington, VA 22217		10. SPONSORING/MONITORING AGENCY REPORT NUMBER

11. SUPPLEMENTARY NOTES The views expressed in this thesis are those of the author and do not reflect the official policy or position of the Department of Defense or the U.S. Government.

12a. DISTRIBUTION/AVAILABILITY STATEMENT Approved for public release; distribution is unlimited.	12b. DISTRIBUTION CODE

13. ABSTRACT (maximum 200 words)

The high resolution DIECAST ocean model, with improved physics, is used to simulate the annual cycle of mesoscale variability in the California coastal region. Model improvements include reduced numerical dispersion, an annual cycle of climatological wind stress forcing enhanced in magnitude near the coastal headlands, and barotropic and baroclinic boundary inflows and outflows. A six year simulation produced results in general agreement with recent observations of the annual cycle in the California Current although the gradients of sea surface temperature and dynamic height are generally stronger, and show more structure than observed. The stronger gradients indicate increased coastal upwelling and produced faster geostrophic currents than observed. A region of maximum Eddy Kinetic Energy (EKE), originally formed in the upper ocean over the continental slope in late spring, migrates westward on a seasonal timescale consistent in magnitude and phase with observations. At the same, the EKE spreads vertically into the deep ocean, decreasing the surface EKE west of about 126°W. This result clearly identifies a non-dissipative process that can account for the pronounced decrease of EKE west of 126°W recently documented in the literature. Deficiencies in the simulation include some artificial influences from the incompletely open western boundary, an exaggerated response of the surface circulation to the Mendocino escarpment and the absence of a significant poleward surface current along the coast in winter.

14. SUBJECT TERMS California Current, Numerical Model, Ocean Variability			15. NUMBER OF PAGES 76
			16. PRICE CODE
17. SECURITY CLASSIFICATION OF REPORT Unclassified	18. SECURITY CLASSIFICATION OF THIS PAGE Unclassified	19. SECURITY CLASSIFICATION OF ABSTRACT Unclassified	20. LIMITATION OF ABSTRACT UL

NSN 7540-01-280-5500

Standard Form 298 (Rev. 2-89)
Prescribed by ANSI Std. 239-18 298-102

SEASONAL VARIABILITY
IN THE CALIFORNIA CURRENT,
A DIECAST MODEL STUDY

Joseph R. Donato
Lieutenant, United States Navy Reserve
B.S., University of New England, 1980

Submitted in partial fulfillment
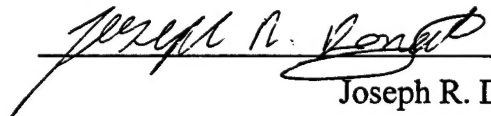of the requirements for the degree of

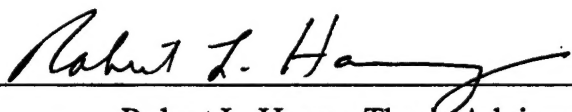## MASTER OF SCIENCE IN METEOROLOGY
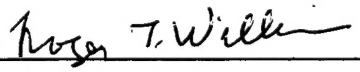## AND PHYSICAL OCEANOGRAPHY

from the

NAVAL POSTGRADUATE SCHOOL
December 1998

Author: _____

Joseph R. Donato

Approved by: _____

Robert L. Haney, Thesis Advisor

_____

Roger T. Williams, Second Reader

_____

Carlyle H. Wash, Chairman
Department of Meteorology

iii

ABSTRACT

The high resolution DIECAST ocean model, with improved physics, is used to simulate the annual cycle of mesoscale variability in the California coastal region. Model improvements include reduced numerical dispersion, an annual cycle of climatological wind stress forcing enhanced in magnitude near the coastal headlands, and barotropic and baroclinic boundary inflows and outflows. A six year simulation produced results in general agreement with recent observations of the annual cycle in the California Current although the gradients of sea surface temperature and dynamic height are generally stronger, and show more structure than observed. The stronger gradients indicate increased coastal upwelling and produced faster geostrophic currents than observed. A region of maximum Eddy Kinetic Energy (EKE), originally formed in the upper ocean over the continental slope in late spring, migrates westward on a seasonal timescale consistent in magnitude and phase with observations. At the same, the EKE spreads vertically into the deep ocean, decreasing the surface EKE west of about 126°W. This result clearly identifies a non-dissipative process that can account for the pronounced decrease of EKE west of 126°W recently documented in the literature. Deficiencies in the simulation include some artificial influences from the incompletely open western boundary, an exaggerated response of the surface circulation to the Mendocino escarpment and the absence of a significant poleward surface current along the coast in winter.

TABLE OF CONTENTS

I. INTRODUCTION

A. BACKGROUND AND OBJECTIVE

The purpose of this study is to describe and analyze a numerical simulation of the California coastal zone using the DIECAST (Dietrich-Center for Air Sea Technology) ocean model, with improved physics (Dietrich, 1997), and to compare the observations/results with recent in-situ and remote sensing observational studies. The study is essentially a continuation of the study conducted by Akahoshi (1995). In Akahoshi's study the DIECAST ocean model did not include a surface wind forcing but did include a simplified surface buoyancy forcing with damping to the Levitus (1982) climatological summertime means of temperature and salinity and an equatorward-flowing surface jet at the northern boundary. Observationally realistic boundary conditions with realistic topography and coastal geometry were also incorporated into Akahoshis' model study. In his paper Akahoshi concluded that the DIECAST ocean model simulation, utilizing realistic topography and coastal geometry with boundary forcing alone, can produce results that are consistent with observations to the first order. Akahoshi also conjectured that the inclusion of a surface wind forcing and a southern boundary forcing in the form of a

1

poleward-flowing undercurrent would likely bring model results more in line with observations. Akahoshi also stated that all model forcings should include an annual cycle to produce the desired end result. Akahoshi's findings were such that further study of the DIECAST ocean model seemed warranted, hence the incorporation of the improved model physics.

The DIECAST ocean model is a robust, state-of-the-art, high resolution, regional model. Primary strengths of the model include its' ability to generate and resolve fine eddy structure in three dimensions and eddy propagation, and its ability to be relocated to any ocean or lake region with relative ease. The current simulation with the DIECAST ocean model incorporates significantly improved physics over that utilized by Akahoshi (1995). Significant improvements in the simulation include surface wind forcing by the Hellerman and Rosenstein (1983) mean monthly climatological wind fields, an additional coastal wind enhancement (headland winds), surface buoyancy damping to the Levitus (1982) climatological monthly means of temperature and salinity, barotropic inflow and outflow at the northern and southern boundaries, and a baroclinic coastal jet at the northern boundary in phase with the surface winds. A more detailed description of the current version of the DIECAST ocean model can be found in chapter two.

B. PREVIOUS STUDIES

1. Enriquez and Friehe, 1995

In their research, Enriquez and Friehe conducted an analytical and numerical study of the relative importance of wind stress (τ) and the curl of the wind stress ($\nabla \times \tau$) upon coastal upwelling/downwelling and its role in generating circulations near the coast, i.e. the time evolution of the mixed layer depth, h. The geographical location of their study was centered around Point Arena from 38° 12'N to 39° 12'N and from 124° 24'W to the coast. For their study Enriquez and Friehe used aircraft derived wind data from low-level (30 m) flight tracks, and from vertical profiles north of Point Arena and south of the Russian River. The observed data, which showed enhanced wind stress and wind stress curl just offshore and south of Point Arena, was applied to a simple two layer, vertically integrated, linearized, reduced-gravity numerical model of coastal upwelling. The lower layer was dynamically inactive and the motion of the upper layer was represented by the first baroclinic mode. Finite differencing was accomplished on a staggered Arakawa C grid using a leapfrog time advance scheme. No-slip conditions were applied to a 2 km x 2 km square grid coastline. Open boundary conditions existed on the northern, southern, and western boundaries. The analytical model was a simplified version of

3

the numerical model and assumed a straight coastline. No-slip boundary conditions were applied at the coast and finite values of the variables were required far offshore.

Three solutions were obtained from the study - an analytical steady-state solution, an analytical time-varying solution, and a numerical solution. Each solution showed that the application of wind stress curl near the coast had a significant effect on the upwelling/downwelling regime. Specifically, curl not only increased the rate of upwelling and decreased the rate of downwelling but caused the horizontal extent of the effects of upwelling to expand beyond the curl's application area. Additionally, local (neighboring) extreme values of curl tended to merge into smoother large-scale structures with less pronounced peaks. The magnitude of upwelling near the coast was uniform, decreasing farther offshore, and was strongest near areas of wind stress curl maxima.

Sustained high concentrations of positive wind stress curl observed near Point Arena are thought to be caused by the local coastal topography affecting the low-level wind flow. The study showed the importance of such concentrated wind stress to coastal upwelling.

2.   Burk and Thompson, 1996

Burk and Thompson (1996) used this study to document the

4

structure, and to investigate the mesoscale processes involved in the spring/summer time Low Level Jet (LLJ) that flows along the California coast from Cape Mendocino to Point Conception. A mesoscale atmospheric numerical model, Navy Operational Regional Atmospheric Prediction System (NORAPS), as described by Hodur (1987) with a modified physics package as described by Burk and Thompson (1989), was used to conduct the study. Optimum interpolation analysis was used for observational data assimilation. A control experiment was conducted by producing Sea Surface Temperature (SST) fields from the regional Expanded Ocean Thermal Structure (EOTS) and Optimum Thermal Interpolation System (OTIS) as described by Clancy *et al.* (1990).

In their study, Burk and Thompson found that the LLJ had several regions of local maxima along the coast in the lee of capes and points. Associated with these regions of local LLJ maxima or "patches" are areas of enhanced upwelling and cold SST pools produced by the enhanced surface stress maxima caused by the topographically forced LLJ patches.

3. Dorman *et al.*, 1998 (In review)

In their study, Dorman *et al.* (1998) conducted instrumented flight surveys and real-time and retrospective numerical model forecasts of the California coast to determine the correct mesoscale structure of the Marine Boundary Layer

5

(MBL) over the ocean, particularly in the vicinity of Point Sur. Aircraft data was augmented with both fixed station and ocean sensing systems. The Navy's nonhydrostatic Coupled Ocean/Atmosphere Mesoscale Prediction System (COAMPS) was used to provide a larger scale, spatially continuous, three dimensional context of the marine boundary layer structure for the aircraft.

One relevant conclusion of the Dorman *et al.* (1998) study, as it pertains to this study, is that the observed structure of the coastal MBL, supported by the model, is strongly suggestive of an inbound supercritical MBL interacting with the topographic bend in the coast at Point Sur, forming a supercritical expansion fan in the lee (Dorman *et al.*, 1998). Observationally, this correlates with their measurements of the lowest sea surface temperatures being off Point Sur near to, but not exactly under, the wind speed maximum.

4.   Summary

As described in the previous sections, the observational study conducted by Dorman *et al.* (1998) showed that the summertime influence of the subtropical high on the California coast was such that the equatorward flowing geostrophic wind developed a low level, concentrated, atmospheric jet on the leeward side of Point Sur. Dorman *et al.* (1998) theorized

6

that such a feature may also be present at other topographic bends like Cape Mendocino and Point Arena. It is believed that the effect of this feature is such that the enhanced wind stress and its curl locally increase the off-shore Ekman transport and pumping, thereby increasing upwelling and possibly eddy generation and filament formation. As noted previously, the atmospheric model study conducted by Burk and Thompson (1996) supports the existence of these wind jet maxima at all capes and points along the California coast. Figure 1.0 is a representative forecast from their study of surface wind stress maxima in the lee of points and capes along the California coast. Figure 1.1 is the low level wind field around Point Arena from the study by Enriquez and Friehe (1995). The complete significance of such enhanced headland winds for the ocean is still unknown however, and further study needs to be conducted before definitive conclusions can be reached. The primary questions that need to be answered are; 1) Does the enhanced wind feature really exist at every promontory and cape? 2) What is the proper structure or shape of the headland wind jets? 3) What is the proper orientation of the jets? 4) What is their appropriate magnitude? 5) How do these features change seasonally, temporally, and/or diurnally? 6) How significant is this feature in the over all coastal dynamics?
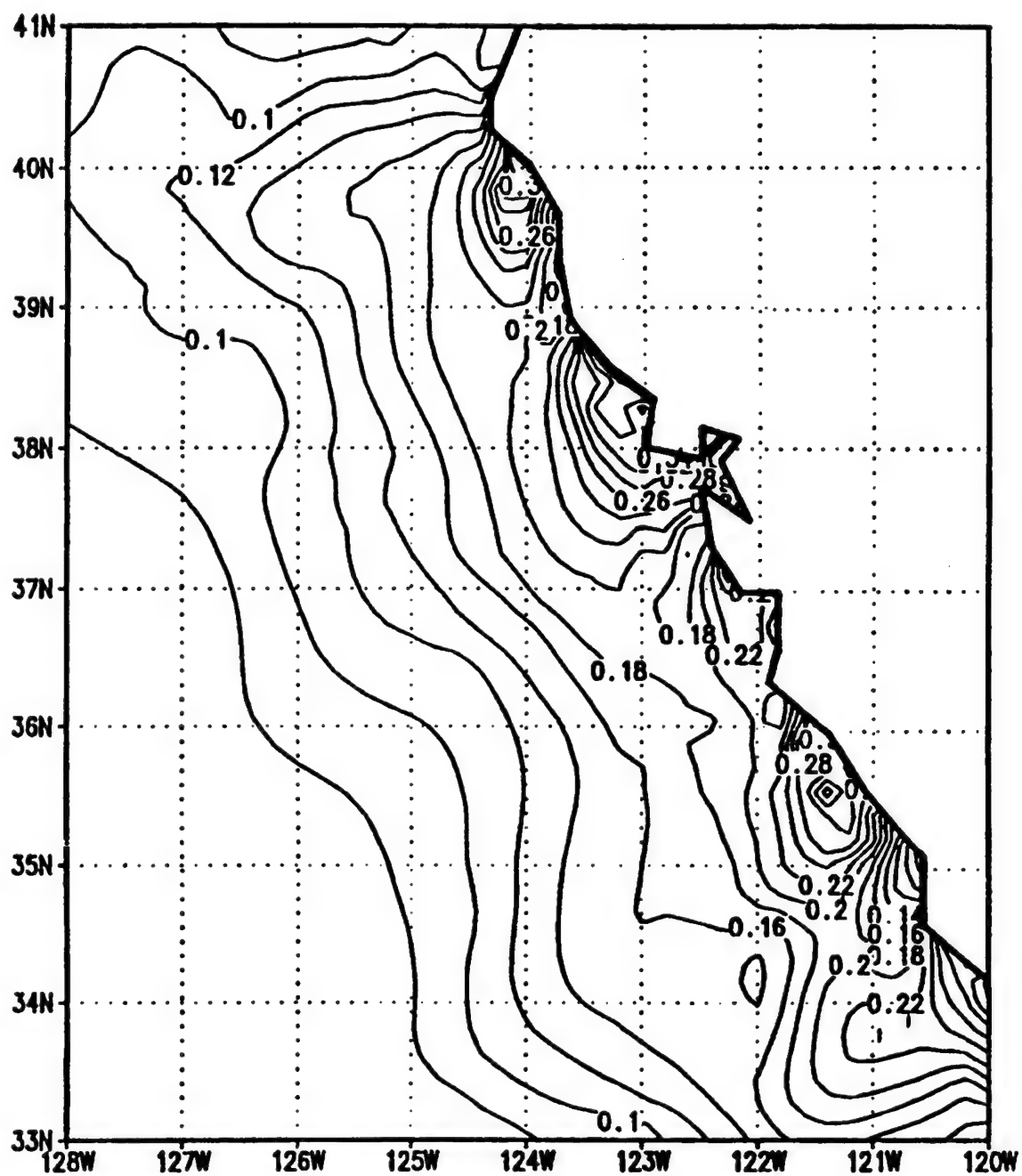
Figure 1.0 – Twelve-hour forecast of surface stress (N m^{-2}) valid 1700 PDT 21 July 1992 (contour interval is 0.02 N m^{-2}). From Burk and Thompson (1996).
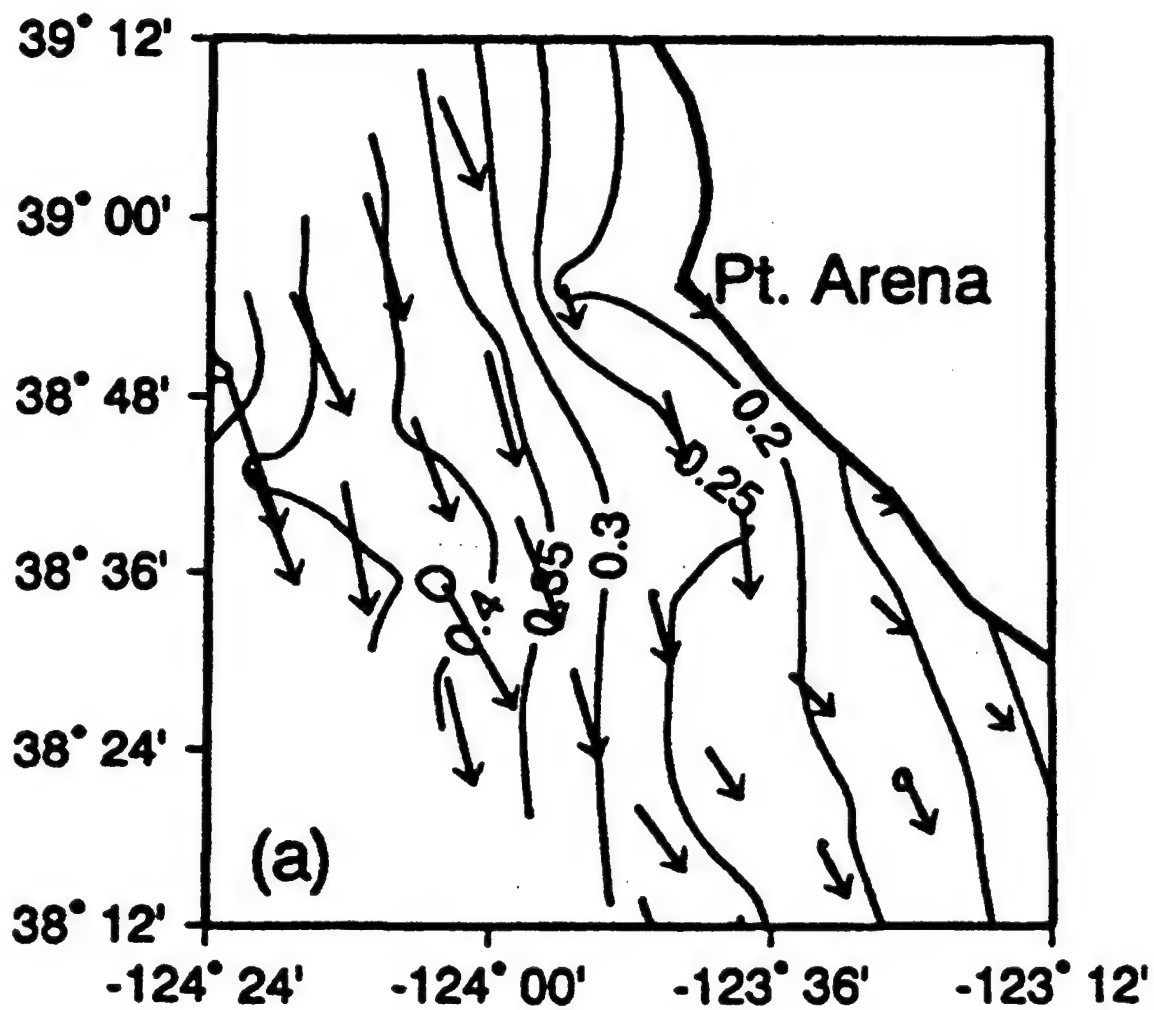
8

Figure 1.1 – Computed wind stress in pascals. Contour interval = 0.05 Pa. From Enriquez and Friehe (1995).

The present study, utilizing an idealized form of these strong coastal winds, is the first one to specifically address the question of their importance in forcing the coastal ocean.

II. MODEL DESCRIPTION AND CONFIGURATION

The following discussion provides a description of the DIECAST ocean model and its configuration for the simulation being studied.

A. DIECAST MODEL

The DIECAST ocean model is a primitive equation, z-level ocean/lake circulation model (Dietrich, 1997). It is hydrostatic, incompressible, rigid-lid, partially implicit, and fully conservative. The model is robust with real (unfiltered) topography, has very low (realistic) dissipation, and incorporates full thermodynamics.

The model uses a pair of colocated grid structures for maximum computational accuracy and minimal numerical dispersion. An Arakawa A-grid is used for all computations of advection, diffusion, friction, Coriolis, and baroclinic pressure gradient forces. This greatly reduces numerical dispersion for the Coriolis term and a fourth order pressure gradient calculation improves it's accuracy on the A-grid. Velocity is then interpolated by a fourth order method to an Arawaka C-grid structure where boundary velocity updates, incompressibility constraint calculations and removal of the vertically integrated divergence are accurately and efficiently performed. Velocity values are then interpolated

back to the Arawaka A-grid. This improvement to the DIECAST ocean model, compared to the study by Akahoshi (1995), results in far less numerical dispersion with a much improved handling of eddies and fine scale gradients.

B. MODEL CONFIGURATION

1. Domain

The domain of the model is from 32.0°N to 42.0°N and from 132.5°W to the coast. To remove possible boundary influences on the analyzed fields, the analysis domain has been confined to the region from 34.5°N to 41.0°N and from 128.0°W to the California coast. This extends from Point Conception to just north of Cape Mendocino and from the California coast to about 600 km offshore. The coastline topography includes the major headlands of Cape Mendocino, Point Arena, Point Reyes and Point Sur (see Figure 2.0). These headlands will become an important topic of discussion below.

2. Resolution

The longitudinal/horizontal resolution of the model is locally fixed at $\frac{1}{12}^o$ longitude. Latitudinal resolution is variable such that the grid spacings are equal, $\Delta x = \Delta y$, where $\Delta y = \frac{\sim 111\ km}{12} \times \cos(lat)$. This approximately equates to $\Delta x = \Delta y = 7.62\ km$ at 34.5°N and $\Delta x = \Delta y = 6.98\ km$ at 41.0°N. The model has 20 vertical layers of resolution with the uppermost layer being 21 m thick and expanding down to a 689 m bottom

12

Model Domain Topography

3.01e+003

2.49e+003

Cape Mendocino

Point Arena

3.64e+003

491

3.64e+003

3.64e+003

Point
Sur

40

39

38

37

36

35

Latitude (Degrees North)

-128   -127   -126   -125   -124   -123   -122   -121
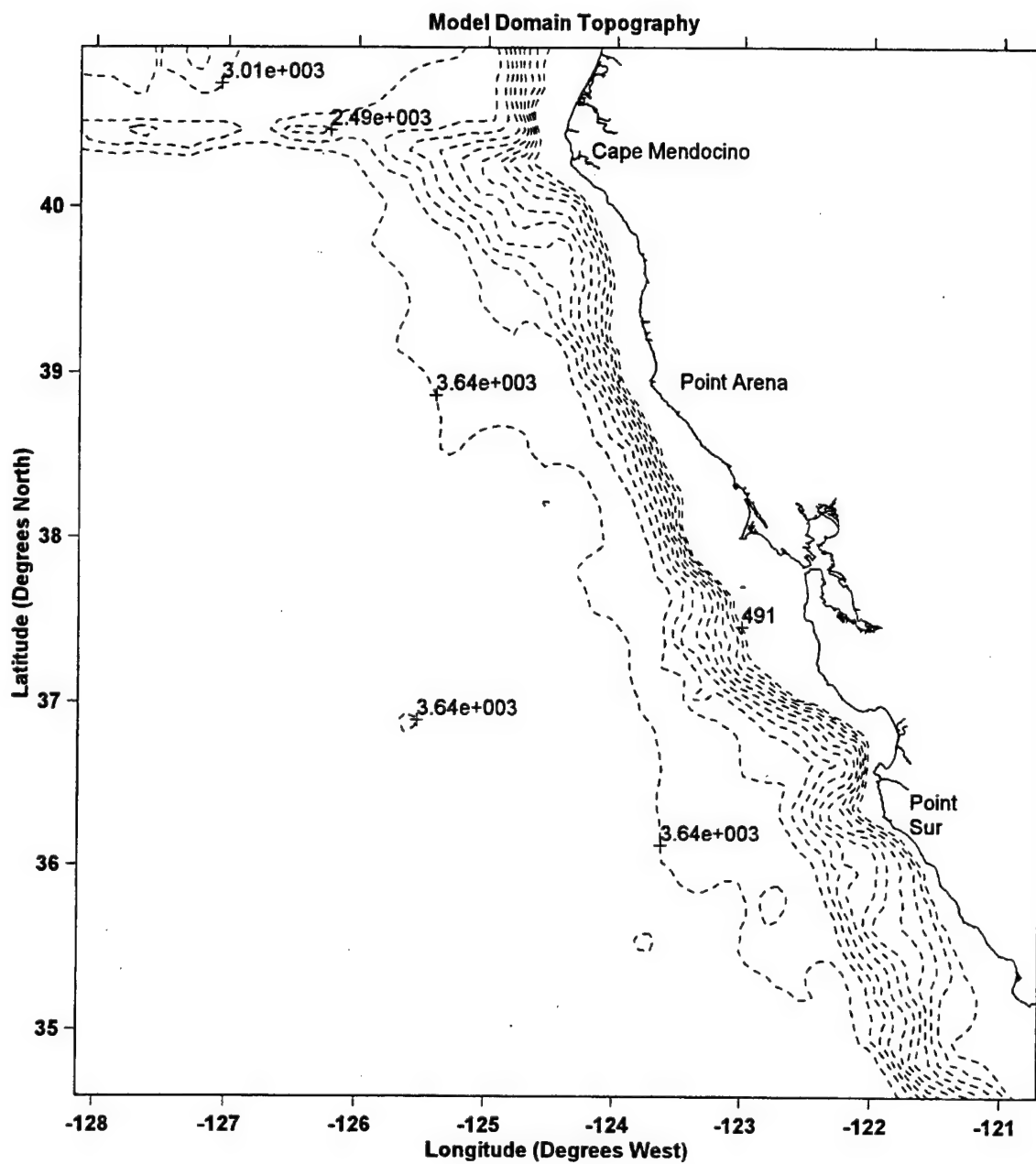
Longitude (Degrees West)

Figure 2.0 – Analysis domain depicting model topography levels
10 through 20. Levels one through nine were omitted to reduce
clutter. Depth is in meters.

layer thickness (see Table 2.0).

layer	z(m)	Δz(m)	layer	z(m)	Δz(m)
1	10	21	11	612	132
2	33	25	12	756	158
3	61	30	13	930	200
4	94	37	14	1139	219
5	134	44	15	1389	275
6	182	52	16	1691	330
7	239	63	17	2053	397
8	308	76	18	2488	478
9	392	91	19	3011	573
10	492	110	20	3640	689

Table 2.0 - Model layers with corresponding depth in meters.
Δz is the layer thickness in meters.

Higher resolutions in the upper ocean, i.e. smaller
vertical depth differences, were designed to resolve the
larger vertical gradients present in the upper ocean. In
general, the high vertical resolution provides for a more
realistic representation of topography (see Figure 2.0). The
coastline and bottom depths were derived from the ETOPO-5
topographic data sets (NOAA, 1986).

3. Surface Forcing

a. Climatological Surface Winds

The climatological surface wind stress forcing comes
from the Hellerman and Rosenstein (1983) data base, which

gives monthly averaged stress components. These are interpolated to the model's grid using a multi-quadratic interpolation scheme. The monthly values are interpolated in time to daily values and then modified by an idealized headland wind enhancement (below) to define the total wind forcing at the surface.

b. Headland Winds

In the present simulation, an idealized enhancement of the surface wind stress in the vicinity of the coastal headlands is added to the climatological wind stress to provide the total wind stress forcing in the simulation.

To do this, a headland wind enhancement factor is constructed by accumulating an idealized representation of the individual effect of each of four headlands (Cape Mendocino, Point Arena, Point Reyes, and Point Sur) on the surface stress. The resulting model wind stress is given by

$$\tau = \tau_c (1 + A(t) \, F(x,y)),$$

where τ_c is the monthly mean climatological wind stress of Hellerman and Rosenstein (1983) as described in the previous section, $A(t)$ is the time-varying normalized amplitude of the additional headland wind effect and $F(x,y)$ is its spatial pattern. Thus, the headland wind effect is a simple time- and space-dependent scalar enhancement of the climatological wind stress. This enhancement therefore does not change the wind

15

stress direction, which remains the same as T_c. To match what is currently known about the observed headland wind phenomena (Rogers *et al.*, 1998), the normalized amplitude function A(t) is specified to be non-zero only during the warm season of the year, March through September with a peak in May/June, the time of the strongest equatorward winds (Figure 2.1a). Also following observations, the spatial amplitude function F(x, y) is modeled using a Gaussian-like function centered just south of each headland. The spatial spreading and orientation of the fan-like wind patch is controlled by varying the length scales downstream of the headland. The enhancement function F(x,y), which describes the cumulative effect of all four headlands, is shown in figure 2.1b where the individual contribution from each of the four headlands is clearly seen. Since Point Arena and Point Reyes are sufficiently close to one another, the effects of these two headlands combine to give the greatest total wind enhancement off San Francisco Bay. The model wind stress in May/June is therefore up to 2.3 times T_c in that area. Figure 2.2 shows the resulting total surface wind stress fields at four representative times of the year.

c. *Surface Buoyancy Damping*

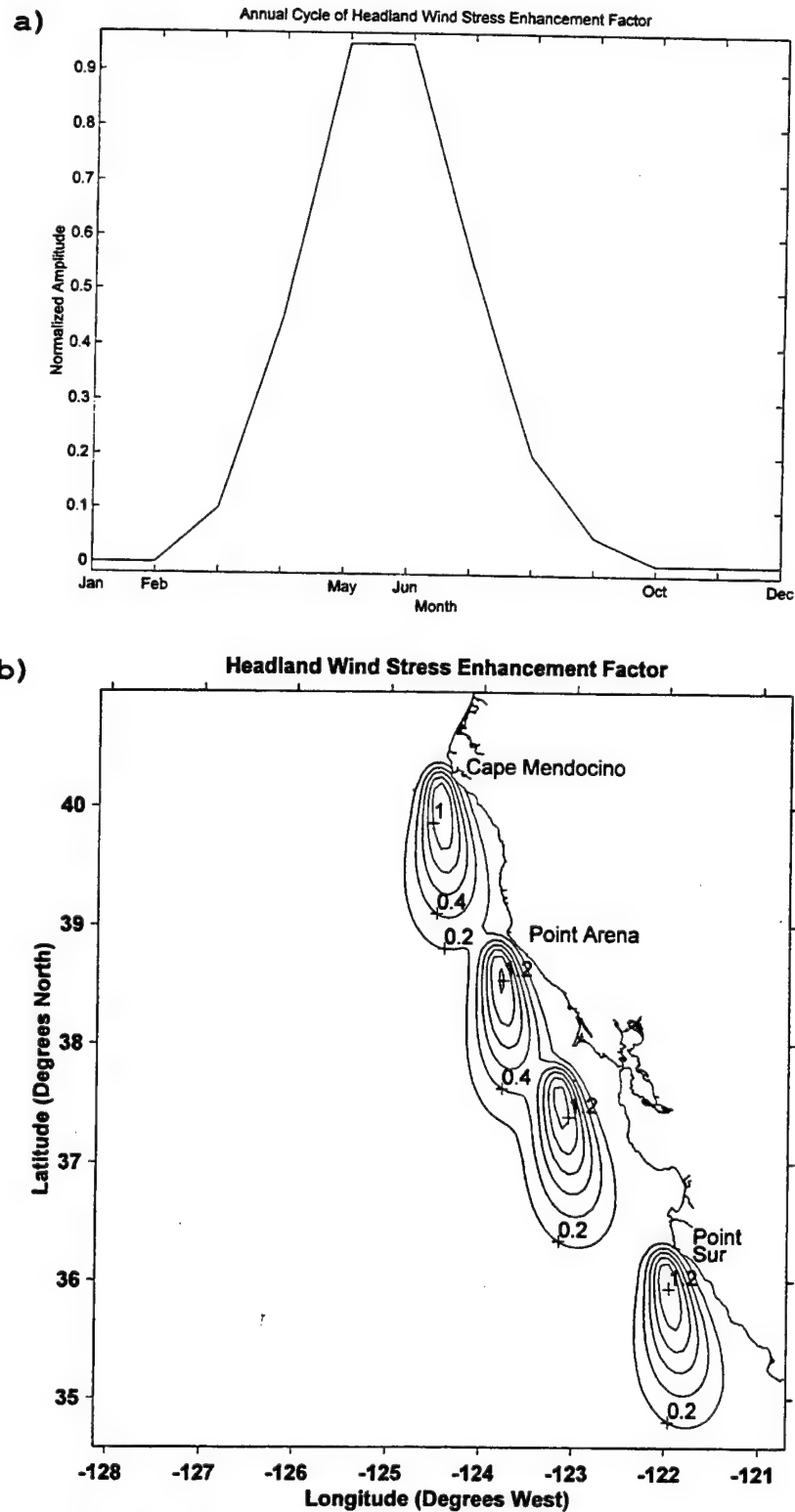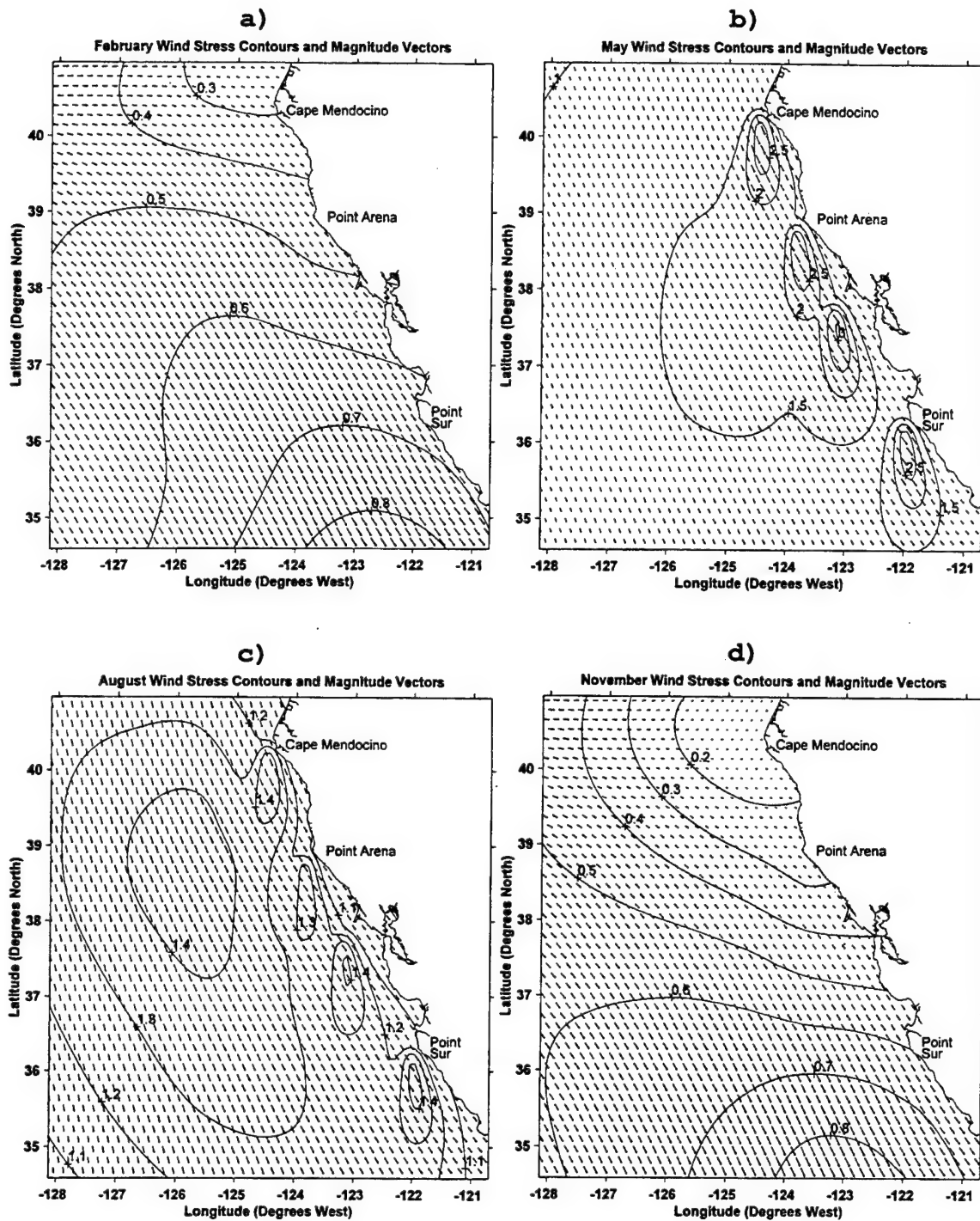Surface buoyancy forcing is very much simplified and

16

Figure 2.1 – a) Monthly change in amplitude of headland wind stress factor. b) Magnitude and structure of headland wind stress factor. Non-dimensional units.

consists of damping the surface fields of temperature and salinity back to the annual cycle of climatological Levitus (1982) values on a time scale of 60 days. McCreary *et al.* (1991) observed that doubling the damping time scale from 40 to 80 days in his model study produced similar results, while only taking longer for his model to reach equilibrium. Thus, the exact value of the damping time scale used is not considered to be critical to the solution.

Numerical damping of all fields is accomplished with a simple diffusion coefficient of 10^5 cm^2/s which increases by 50% in a weak sponge zone at the western boundary. Tangential velocities near the boundary are also damped. Additionally, a weak biharmonic filter is applied to the barotropic velocity and the density field in order to suppress $2\Delta x$ waves.

4. Lateral Forcing and Boundary Conditions

All boundaries are partially open with the computed normal boundary velocity (NBV) determining inflow and outflow. On the western boundary, outflow of Rossby waves is enhanced by adding an additional 1 cm/sec apparent outflow when determining the inflow/outflow condition. In all cases temperature and salinity are advected in or out, and momentum is damped as noted above. Initially, NBV is the specified normal boundary velocity, but during the simulation NBV is continually nudged towards the annual cycle of specified

Figure 2.2 - Surface wind stress contours and vectors. Units are dynes per cm²: **a)** February, contour interval 0.1 d/cm², **b)** May, contour interval 0.5 d/cm², **c)** August, contour interval 0.1 d/cm², **d)** November, contour interval 0.1 d/cm².

19

velocities on a 15 day time scale. The specified boundary values of normal velocity consist of several parts. The basic velocity is the normal geostrophic baroclinic current computed from the annual cycle of temperature and salinity on the boundary given by Levitus (1982).

A specified barotropic flow is added to the above geostrophic velocities at both the northern and southern boundaries. The barotropic normal velocities are composed of smoothly fitted values taken from the general circulation model of Semtner and Chervin (1992). The Semtner and Chervin model shows an annual cycle of barotropic flow through the California Current, northward in the summer and southward in the winter (Figure 2.3). In this study, the across-boundary barotropic transport is confined to the continental slope and modeled as a sinusoidal oscillation over the annual cycle with an amplitude of 5 Sv and a mean of zero.

In the surface layer, the wind driven Ekman flow is allowed full freedom to change outflow. For subsurface layers the western and northern boundaries are constrained so that the mean value for each layer varies with the annual cycle boundary means. Each subsurface layer is also constrained to have no net divergence.

5. Coastal Jet Forcing

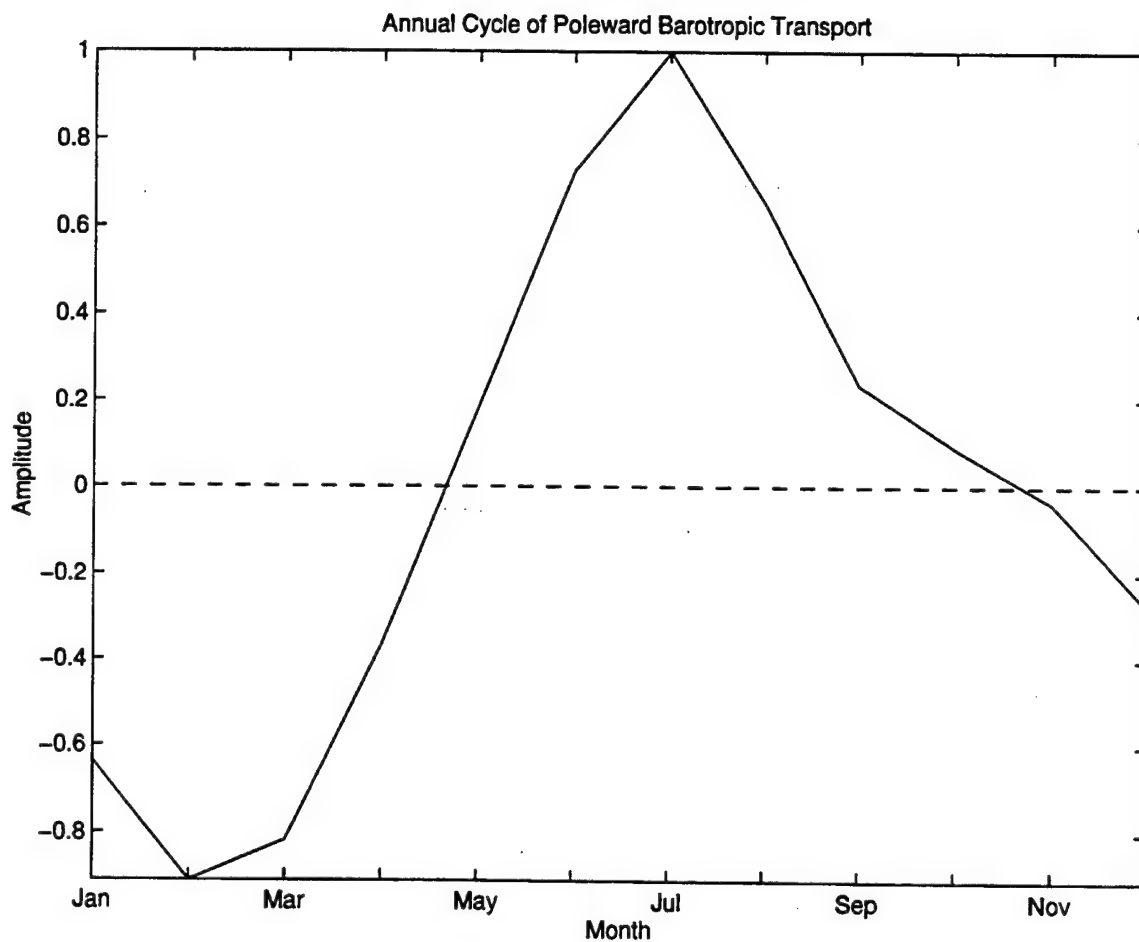At the northern boundary, the Levitus (1982)

Figure 2.3 - Annual cycle of barotropic flow through the California Current. Normalized curve of applied values.

21

climatological temperature and salinity forcing, and the resulting geostrophic velocities described above, are modified to include an observationally realistic equatorward-flowing upper ocean jet. This is accomplished by adjusting the vertical sections of Levitus temperature and salinity at the boundary. Figure 2.4 shows the resulting adjusted climatological temperature, salinity and v component of velocity at 42.0°N averaged over the month of May, the period of peak intensity and the month of November, an opposing month of relatively weak intensity. The jet (Figure 2.4c) is structured as a Gaussian jet with a core velocity of 30 cm/s, a horizontal scale of about 95 km, and a vertical scale of about 750 m. It is positioned adjacent to the continental slope in about 3000 m of water. The jet structure is intended to approximate the coastal jet observed in June 1987 during the Coastal Transition Zone (CTZ) experiment (Kosro et al., 1991). The time variation of the coastal jet (Figure 2.5) is prescribed to match the annual cycle of the baroclinic jet in the California Current as found in the Semtner and Chervin (1992) simulation that was also forced by the Hellerman and Rosenstein (1983) wind stress. The coastal jet is prescribed simply for consistency at the boundary, since we expect such a coastal jet to be generated immediately inside the domain in response to the wind forcing.
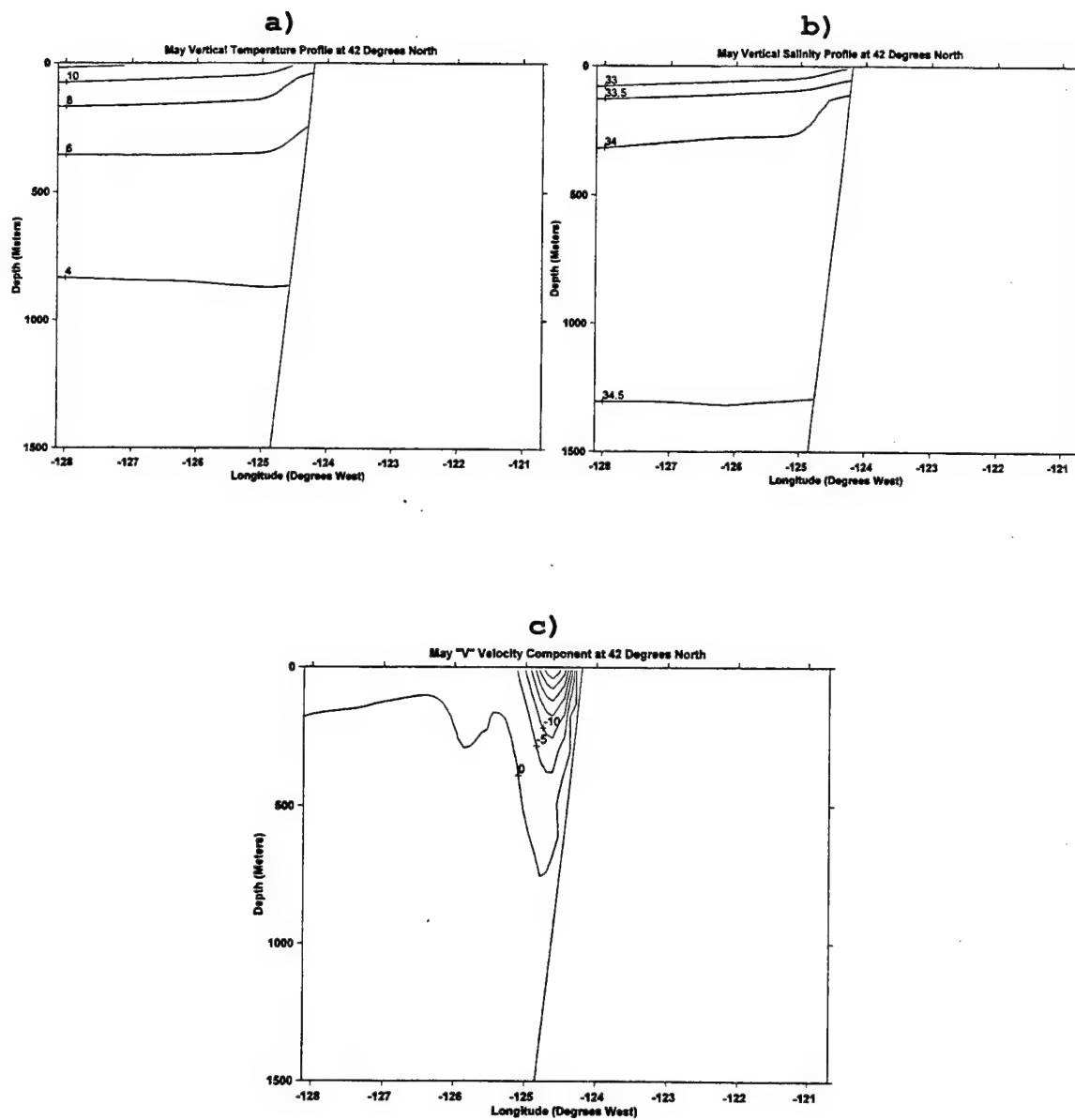
a)

May Vertical Temperature Profile at 42 Degrees North

b)

May Vertical Salinity Profile at 42 Degrees North

c)

May "V" Velocity Component at 42 Degrees North

Figure 2.4(a-c) – Boundary conditions at 42° north for the month of May. **a)** temperature (°C), **b)** salinity (psu), **c)** v velocity component (cm/s).

23

d)

November Vertical Temperature Profile at 42 Degrees North

e)

November Vertical Salinity Profile at 42 Degrees North

f)
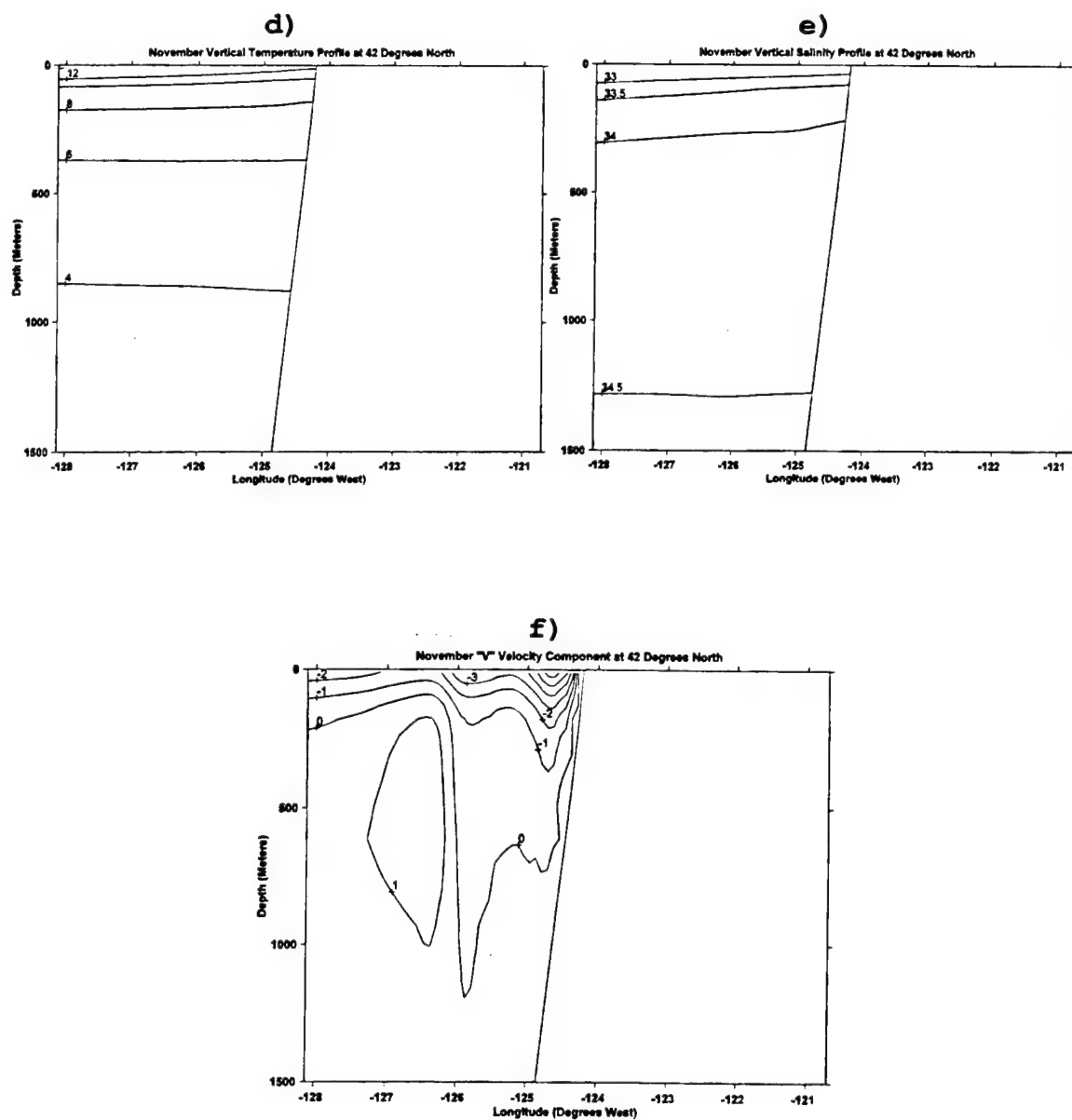
November "V" Velocity Component at 42 Degrees North

Figure 2.4(d-f) - Boundary conditions at 42° north for the month of November. **a)** temperature (°C), **b)** salinity (psu), **c)** v velocity component (cm/s).
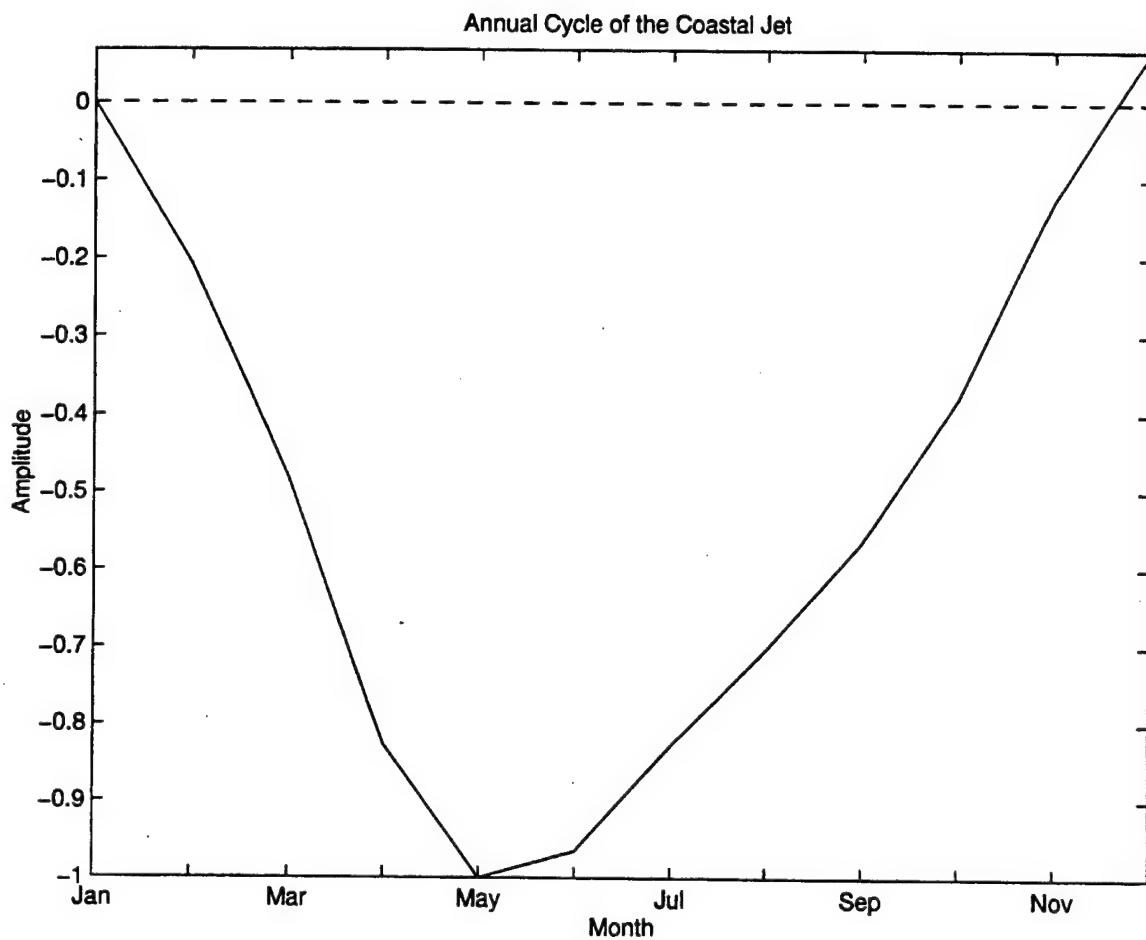
Figure 2.5 – Time variation of baroclinic jet at the northern boundary.   Normalized curve of applied values.

6.   Time frame

The model was run for a total time period of six model years. Initial conditions consisted of one degree resolution climatological monthly means of temperature and salinity from Levitus (1982). This data was interpolated and gridded to our models matrix to provide a full field of T,S values for the initial January 01 start time. As described above, the monthly values of T,S on the lateral boundaries (adjusted to produce the coastal jet at the northern boundary) were then used to force the annual cycle. In addition, the surface values were used to provide the annual cycle for surface restoration.

The first year of the model run was considered to be the spin-up period while years two through six were considered to be in near-equilibrium. Figure 2.6, a time series plot of the daily mean eddy kinetic energy at the surface, clearly shows the rapid adjustment period during year one and the slightly downward sloping trend in energy levels from years two through six. Because of this trend the model was considered in near-equilibrium during years two through six and this constituted the majority of the analyzed data fields.
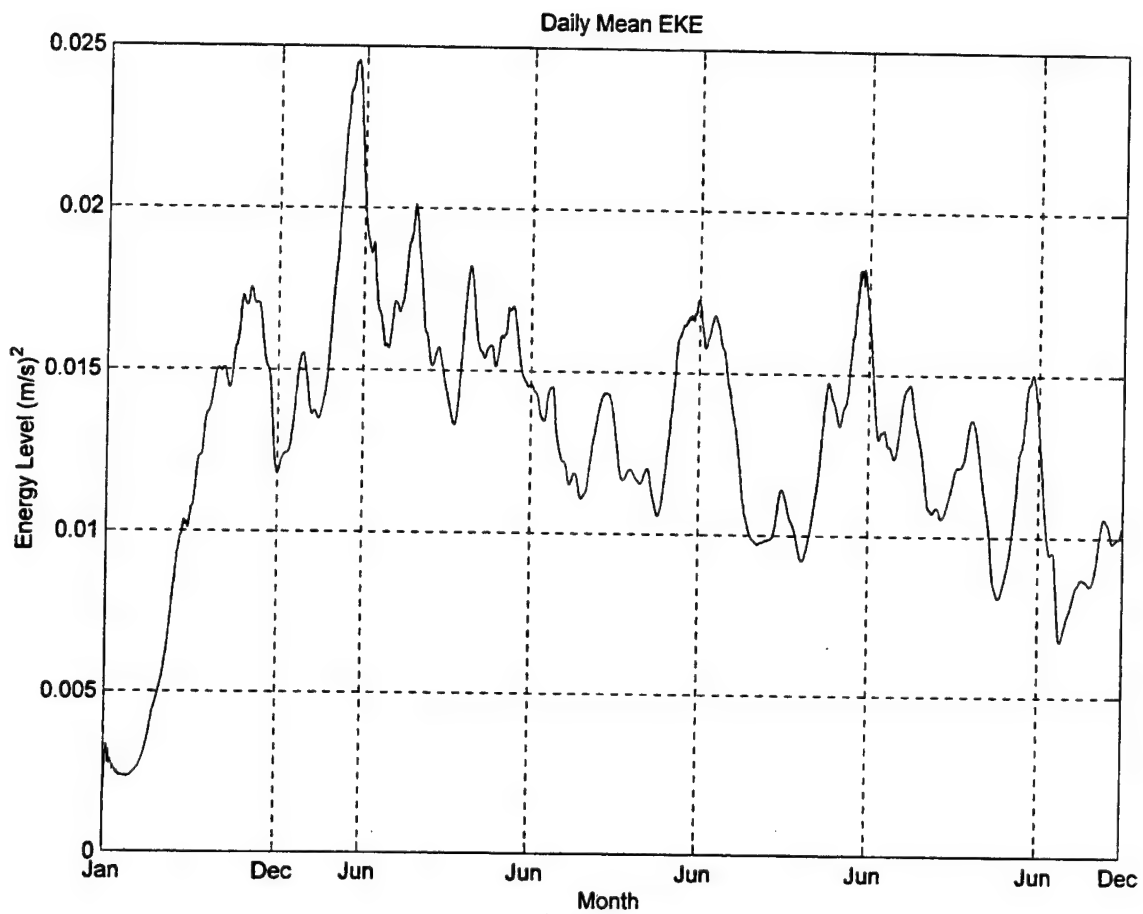
Figure 2.6 – Daily mean Eddy Kinetic Energy at the surface. Units in $(m/s)^2$.

27

III. SURFACE VARIABILITY

This chapter will analyze the model simulated surface variability and compare the results to observations. Specifically, the characteristics of dynamic sea surface height and eddy kinetic energy will be studied and compared to a recent comprehensive observational study conducted by Kelly *et al.* (1998).

A. DYNAMIC SEA SURFACE HEIGHT

The resulting five year mean dynamic sea surface height (SSH) from the simulation (Figure 3.0) shows equatorward geostrophic flow throughout the region, with the broad California Current well offshore and the largest SSH gradients near the coast from north of Point Arena to south of San Francisco Bay. The SSH field has a minimum value of approximately -0.12 m just north of Cape Mendocino near 41°N, 124.5°W and a maximum value of 0.12 m near 34.6°N, 128°W giving a total SSH difference of 0.24 m. Kelly *et al.* (1998) observed a SSH minimum near 36°N, 123°W (see Figure 3.0) with a SSH difference of 0.22 m over the same domain.

A significant difference in the model study compared to observations is the tight gradient of SSH contours that run parallel, and close, to the coast. The -0.12 m contour runs adjacent to the coast from the northern boundary down to
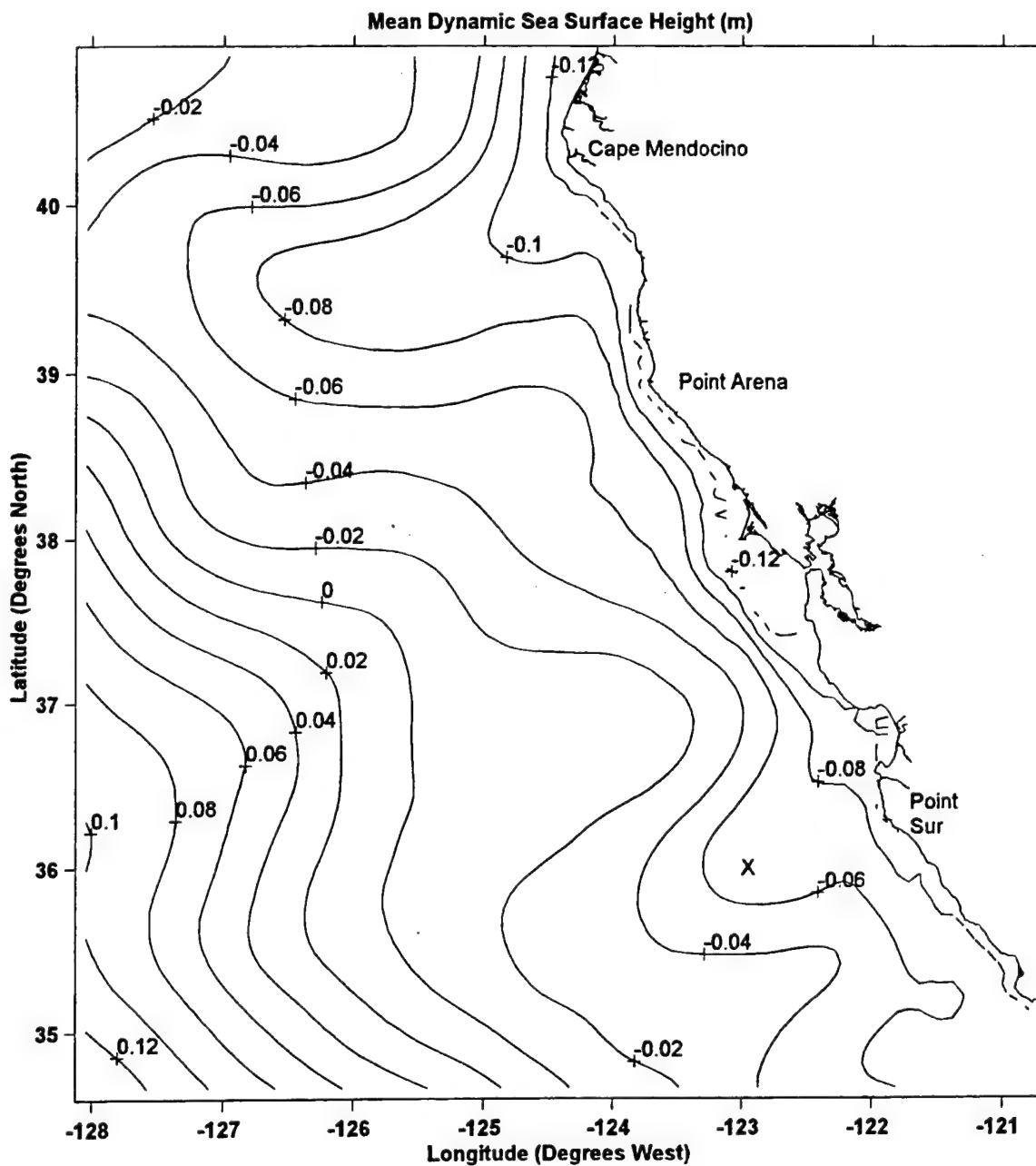
29

Figure 3.0 – Mean Dynamic Sea Surface Height, in meters. Contour interval is 0.02 m. The "X" near 36°N, 126°W marks the location of minimum sea surface height observed by Kelly *et al.*, 1998.

37.3°N, just south of the San Francisco Bay area and the -0.1 m contour runs parallel to it from about 39.5°N to about 36.3°N, just west of Point Sur. The -0.08 m contour begins its run near 39.4°N and goes southeast down the coast to the eastern boundary. There is a large trough, or sea surface depression, extending from Cape Mendocino southwest to about 39.5°N at the western boundary. A smaller rise and depression pair appear southwest of Monterey Bay. This pattern is in contrast to Kelly's findings for the mean SSH in which a single minimum value is located along the coast just west of Monterey Bay with rather uniformly spaced SSH contours generally parallel to the coast but arching cyclonically around the minimum. The deep trough in the simulated SSH field south of the Mendocino escarpment is simply not seen in the observed field.

Comparison of the model mean dynamic sea surface height (Figure 3.0) with the model mean sea surface temperature (SST) field (Figure 3.1) shows a high positive visual correlation between SSH and temperature, especially near the coast and west of the Monterey Bay and Point Sur regions. Particular patterns to observe are the troughing south of Cape Mendocino and west of Point Sur and the ridging west of Point Arena and Monterey Bay. The minimum SST is located along the coast, coinciding with the minimum SSH as expected with coastal
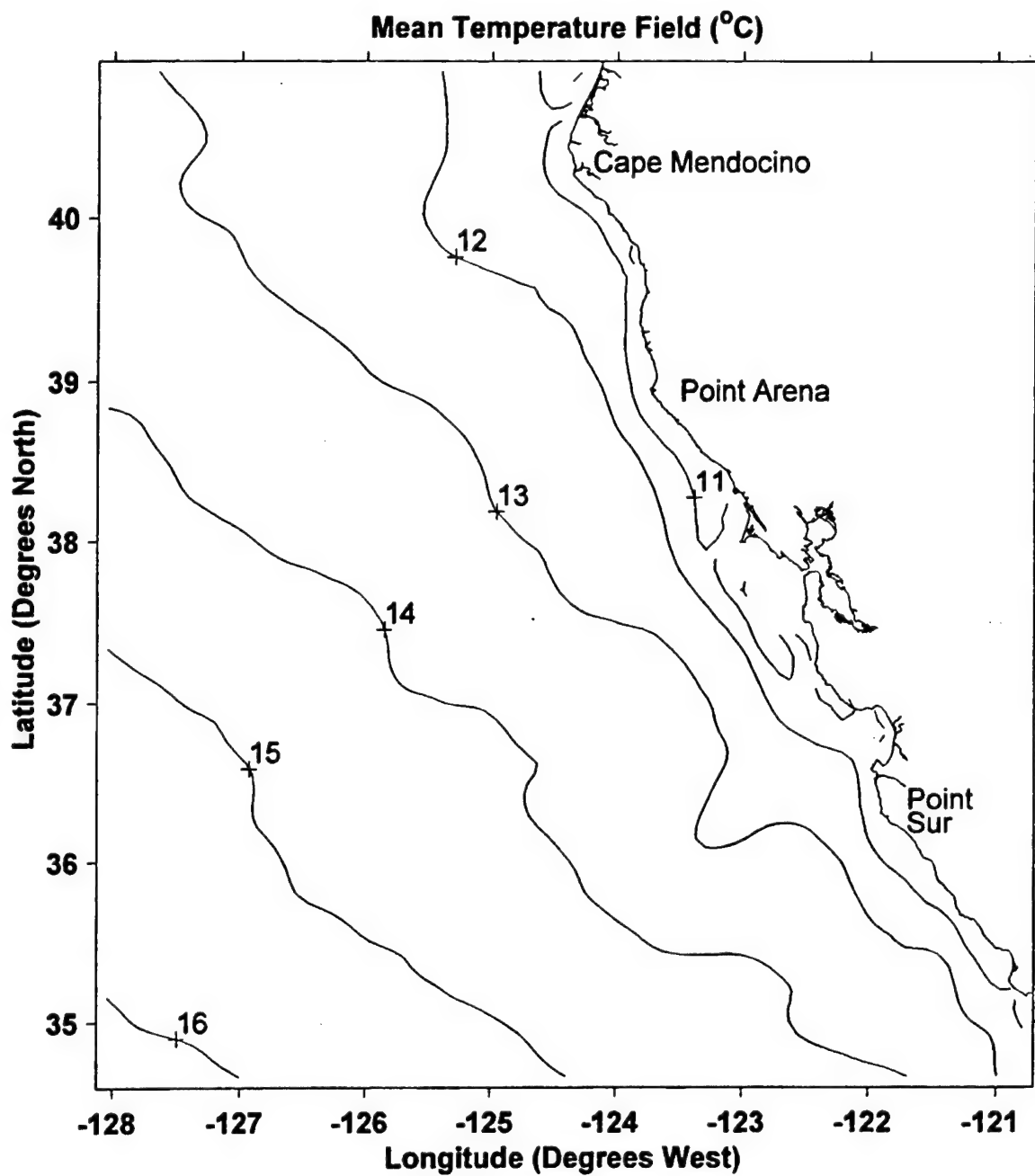
31

Mean Temperature Field (°C)

Figure 3.1 – Mean Sea Surface Temperature in °C. Contour interval is 1°C.

upwelling. Seasonal comparisons of sea surface height and temperature will be conducted in the next section.

The strongest mean geostrophic currents, computed from the mean SSH field, run adjacent to the coast from about 39.25°N to about 37.0°N reaching a maximum velocity of about 0.40 m/s near 37.25°N, 122.75°W. This compares to Kelly *et al.* (1998) who observed a predominately southeastward one year mean geostrophic jet, computed from drifter and hydrographic data, centered along approximately 36°N, 125°W to roughly 31°N, 122°W, with a maximum southeastward velocity of about 0.13 m/s at 36°N, 126°W. At 37°N, 125°W, the maximum observed mean geostrophic velocity is southwestward at about 0.09 m/s. Thus, the model simulated mean surface current maximum of 0.40 m/s is at least three times larger than the maximum observed mean value computed from combined surface and drifter data and climatological hydrographic data.

1.   Combined Seasonal Dynamic Height and Temperature

For this study the seasons are defined as follows: Winter (January, February, March); Spring (April, May, June); Summer (July, August, September); Fall (October, November, December). The following discussion, referring to Figure 3.2a-d, shows the colored temperature field overlain with contoured dynamic sea surface height for each season.

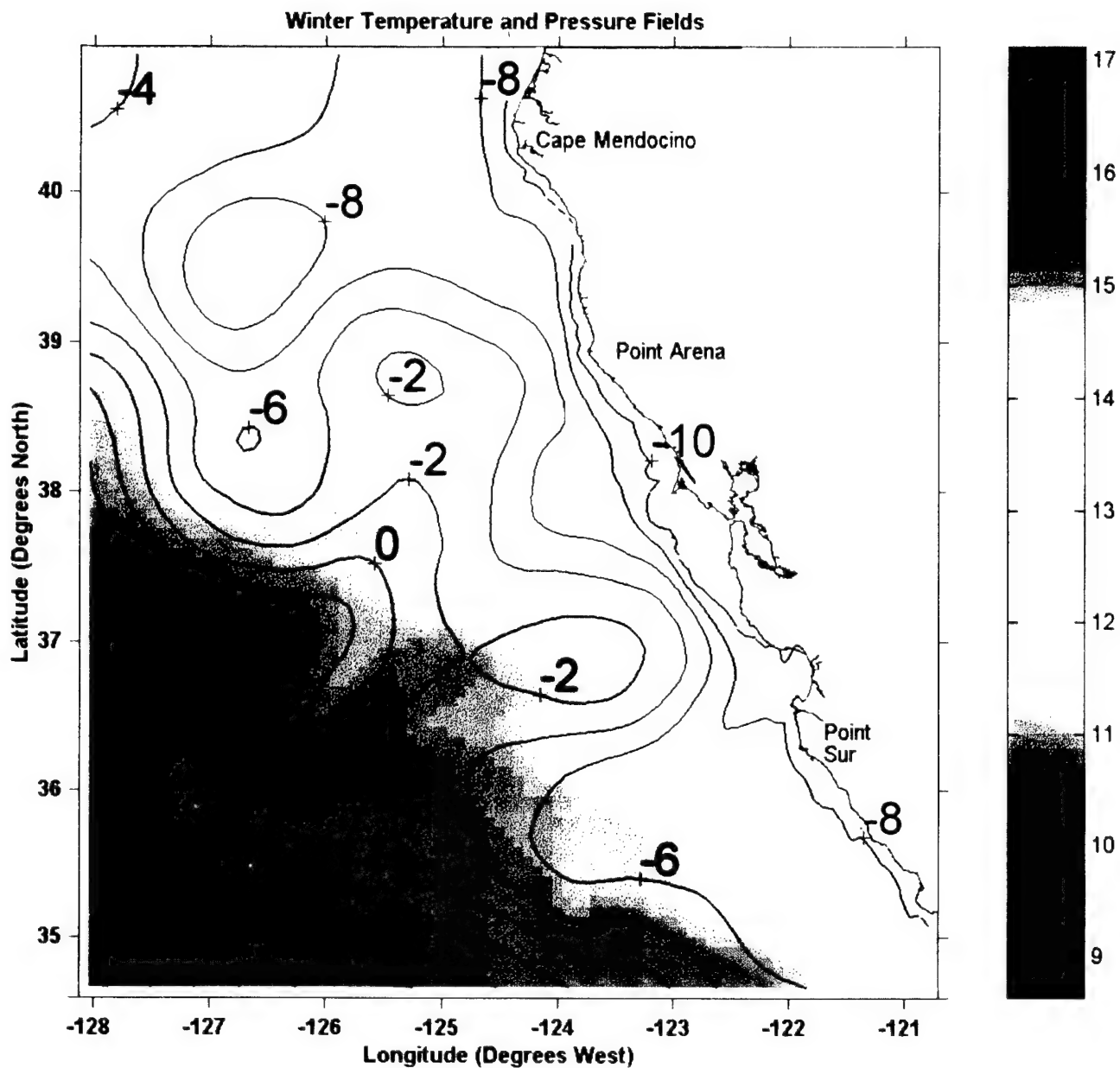Starting with the winter season (Figure 3.2a) one sees

33

Figure 3.2a - Winter temperature field (colored) in °C with the winter surface dynamic height field in cm overlaid. Contour interval is 2 cm.

temperatures in the range of about $11°-12°C$ at the coast, from the northern boundary west of Cape Mendocino to south of Point Sur, to about $17°C$ near $35°N$, $128°W$. Strong ridging in the temperature and pressure fields is evident originating at about $36.5°N$ and extending toward the east and northeast. Local dynamic height highs are located about 140 km west of Point Arena and Monterey Bay. Troughing in the temperature and pressure fields is also evident extending southwest from Cape Mendocino and from Monterey Bay/Point Sur. A small trough is present immediately west of Monterey Bay. A closed low/cyclone is present near $39.5°N$, $126.5°W$. Right along the coast the dynamic height and temperature fields exhibit a relatively relaxed, weak pattern showing strength only near Point Arena and just south of the San Francisco Bay region. Equatorward flow is evident far offshore in the southwest quadrant and adjacent to the coast. By comparison, Strub and James (1998, in review), who analyzed SSH fields from four years of altimeter data, observed a dynamic low in the height pattern west of Point Arena, without the ridge of high pressure seen there in this study, and a low near $35°N$, $123°W$, slightly to the south of the Point Sur trough in this study. Strub and James observed a total temperature range from about $10°C$ to $15°C$, smaller than observed in this study, but with a similar distribution. Their height gradient was also less

than in this study, 12 cm verses 22 cm, with similar distribution as discussed as above.

During the spring season (Figure 3.2b) both the temperature and the dynamic SSH gradients reach their maximum values - a 7°C southwest SST gradient with a 32 cm southwest dynamic SSH gradient. The coldest upwelled coastal waters only go as far south as about 37°N, increasing in temperature south of that. The cold plume west of Cape Mendocino in the winter has migrated to the coast in spring. The gradient of the western boundary SSH ridge has relaxed significantly however the closed high/anticyclone near 37°N, 124°W, present in the winter season, remains and has intensified by at least 6 cm. The gradient of the troughs, also present in the winter season, extending from Cape Mendocino and from Monterey Bay have increased and a closed high has developed near 35.5°N, 122.5°W from a weak ridge present in the winter season. Upwelling along the coast from Cape Mendocino to Monterey Bay has reached its maximum producing the tightest, most concentrated SSH gradient of the four seasons. Seasonal mean geostrophic velocities along the coast have also reached their maximums of about 36 cm/s just west of Cape Mendocino to about 50 cm/s between Point Arena and the Monterey Bay region. Equatorward flow is more uniform, paralleling the coast near shore from the northern boundary to about 37°N and far off
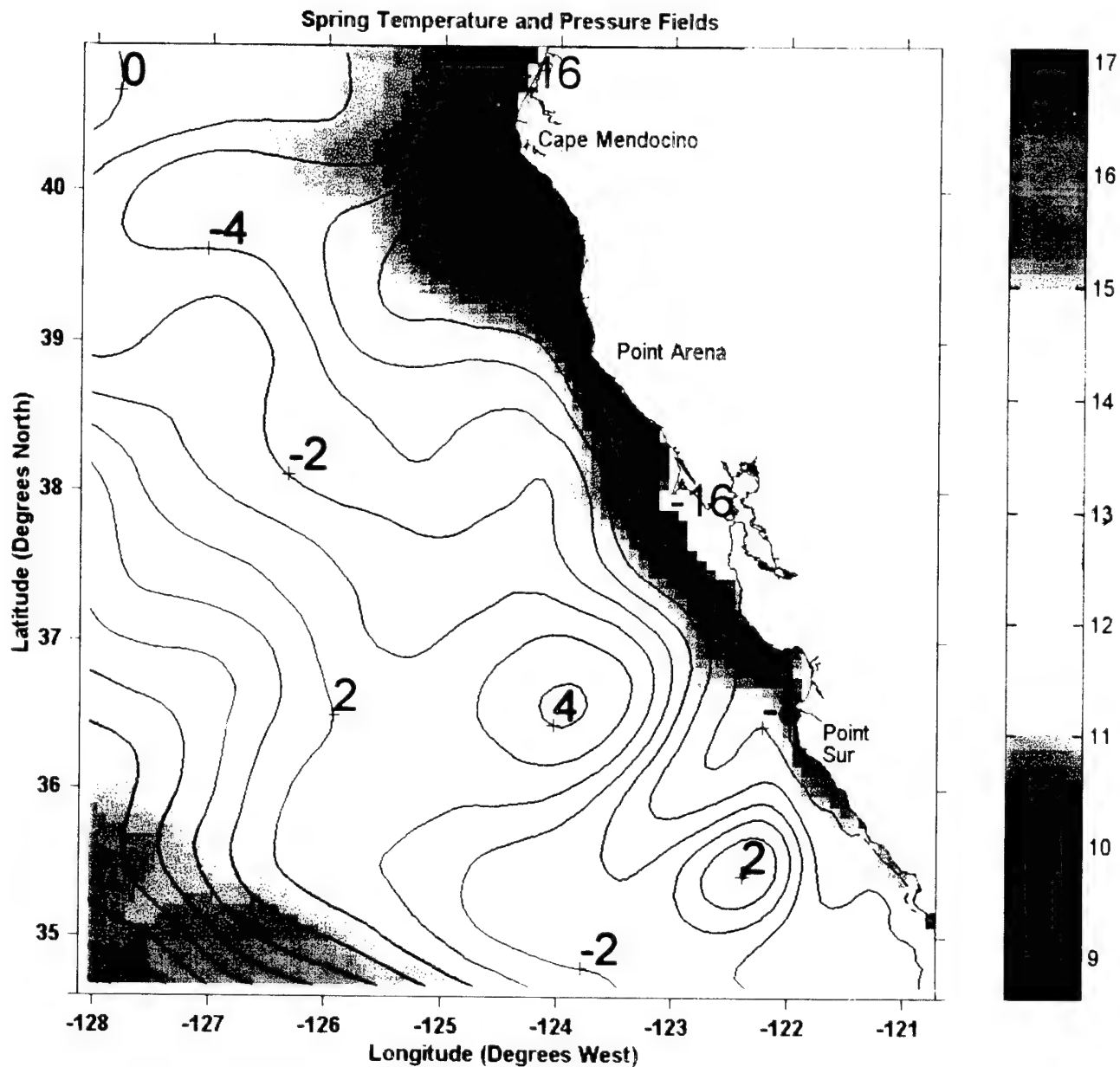
Figure 3.2b - Spring temperature field (colored) in °C with the spring surface dynamic height field in cm overlaid. Contour interval is 2 cm.

37

shore south of 37°N. Again, Strub and James (1998, in review) observed a nearly identical distribution pattern of SST and dynamic SSH, differing from the simulations in the magnitude of the observed gradients – southwest gradients of temperature (about 6°C) and dynamic height (about 20 cm). An approximately 12 cm/s geostrophic flow parallels the entire coast. Again, the model gradients of SSH and the resulting mean geostrophic currents are larger than observed values.

The summer patterns of SSH and SST (Figure 3.2c) have become significantly relaxed compared to the spring patterns. From the coast to well offshore the SST ranges from about 9°-15°C, and the SSH ranges from -14 cm to 10 cm. Upwelling along the coast has become less pronounced though its extent along the coast remains relatively constant. The ridge-trough-ridge pattern west of Point Sur has relaxed considerably from the spring season, suggesting that the strongly seasonal headland wind jet may be the major driving factor. Strub and James observed a similar relaxation of the temperature and height fields but with the coastal jet migrating farther offshore and becoming more diffuse, rather than just weakening in place as seen in the simulation. The observed extent of coastal upwelling has significantly decreased by summer and the coldest temperatures in the upwelling region have slightly increased. The observed
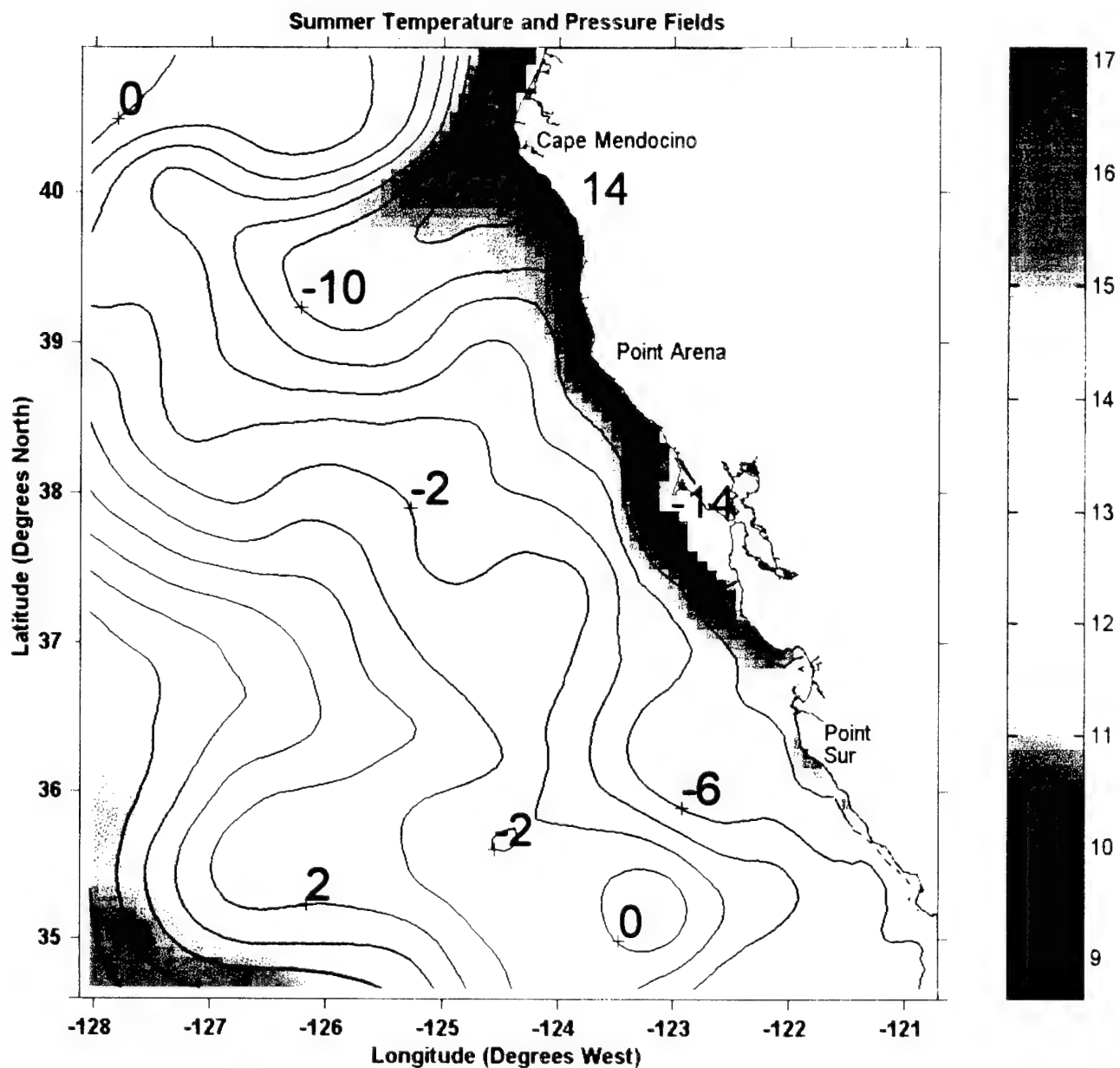
Figure 3.2c - Summer temperature field (colored) in °C with the summer surface dynamic height field in cm overlaid. Contour interval is 2 cm.

temperature range across the domain were about 11°–19°C, somewhat warmer than that found in this model simulation. The mean SSH shows an observed range of about 18 cm in summer, much lower than the 24 cm SSH range found in this simulation.

The observed fields in the fall season (Figure 3.2d) have become completely relaxed showing much less structure and detail than in the previous seasons. Upwelling along the coast has reached its minimum extent, existing only in a small band from Point Arena to Point Sur. The isotherms are distinctly oriented northwest/southeast and range from about 11°C near the coast to 17°C in the southwest. Dynamic SSH ranges from -10 cm along the coast to 12 cm near 34.6°N, 128.0°W. The ridge west of the Monterey Bay remains persistent. The trough south of the Mendocino escarpment near 39.5°N, 126.0°W has closed off and is interacting with a weak coastal ridge slightly off shore adjacent to Point Arena. Strub and James show a similar pattern of relaxation with nearly parallel alignment of the temperature and height fields with the coast. However, the observations show that the coastal jet has weakened and moved farther off shore, resulting in a broader coastal area of cooler temperatures with northward flow developing along the coast from Point Arena to 40.0°N. The model behavior, in which the southward coastal current simply weakens in the fall, is thus different
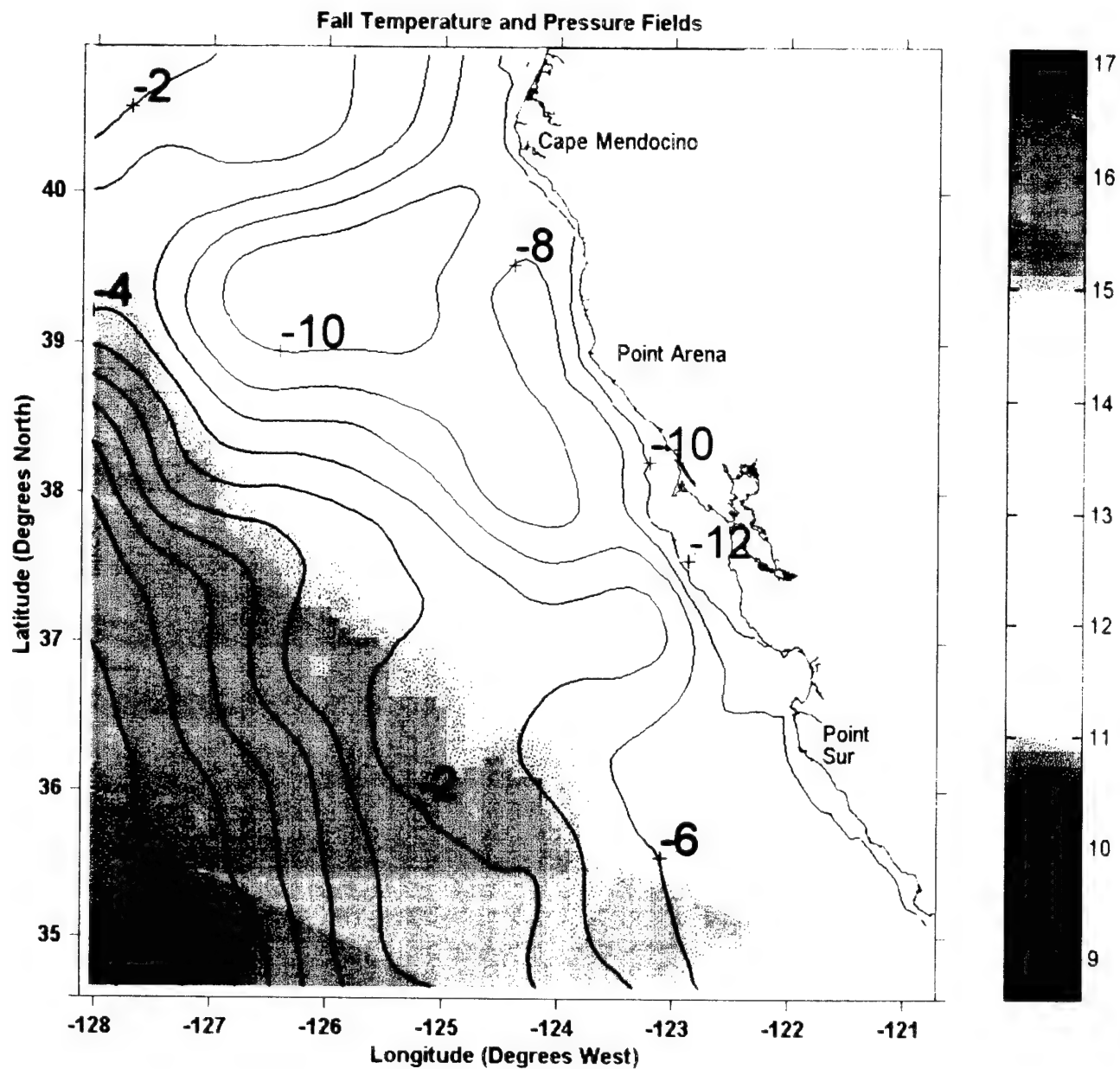
40

Figure 3.2d - Fall temperature field (colored) in °C with the fall surface dynamic height field in cm overlaid. Contour interval is 2 cm.

41

from the observed behavior in which the coastal current propagates offshore. Observed temperature and dynamic SSH ranges in Strub and James are about 7°C and 22 cm respectively, comparable to that of this simulation.

2. Discussion of findings

One difference between our findings and those of Strub and James (1998, in review) is that the model fails to show the seasonal pattern of the coastal jet moving off shore and relaxing from its strongest season, spring, to its weakest season, winter. The model shows a strong coastal jet, essentially from Point Arena to Monterey Bay, with the spring and summer seasons being its strongest, relaxing and retracting through the fall, only to begin strengthening and expanding again in the beginning of spring. This may be a function of the strength and duration of coastal upwelling caused by the idealized headland wind forcing. As noted earlier, this is an area of considerable uncertainty at the present time.

The pattern of substantial ridges and troughs along the coast in the simulation is not so evident in the observational study of Strub and James (1998) where meanders in the along shore flow are much weaker. This may also be a characteristic of the model producing overly strong sea surface temperature and dynamic height gradients causing the resulting strength in

the geostrophic flows to interact with the bottom topography thereby enhancing any natural tendency to ridge or trough (Refer to Figure 2.0). One other possibility for the enhanced features may be artificial influences from the offshore boundary. These possible boundary influences will be discussed further in the next section.

B. EDDY KINETIC ENERGY

1. Mean Kinetic Energy

The mean eddy kinetic energy field (EKE) (Figure 3.3) shows two main regions of relatively high energy at the surface: Region one, located south of Point Arena near $38°N$, $123.5°W$ has a local maximum value of 0.03 $(m/s)^2$ with a sub-region value of 0.025 $(m/s)^2$ about ½ degree latitude to its south; Region two, located south of Point Sur near $35.5°N$, $122.5°W$ has a local maximum value of 0.035 $(m/s)^2$. Minimum values of 0.005 $(m/s)^2$ are located at the northern boundary and along the immediate vicinity of the entire coast. This is in contrast to Kelly *et al.* (1998) who observed a single local maximum value of about 0.045 $(m/s)^2$ farther offshore near $36.5°N$, $125.5°W$ (marked on Figure 3.3) with a minimum contour of 0.015 $(m/s)^2$ along the western boundary from $127.5°W$ to $128°W$. The EKE values shown in Kelly *et al.* (1998) are based on three years of surface drifter data which unfortunately only sampled the region seaward of $124°W$. The EKE
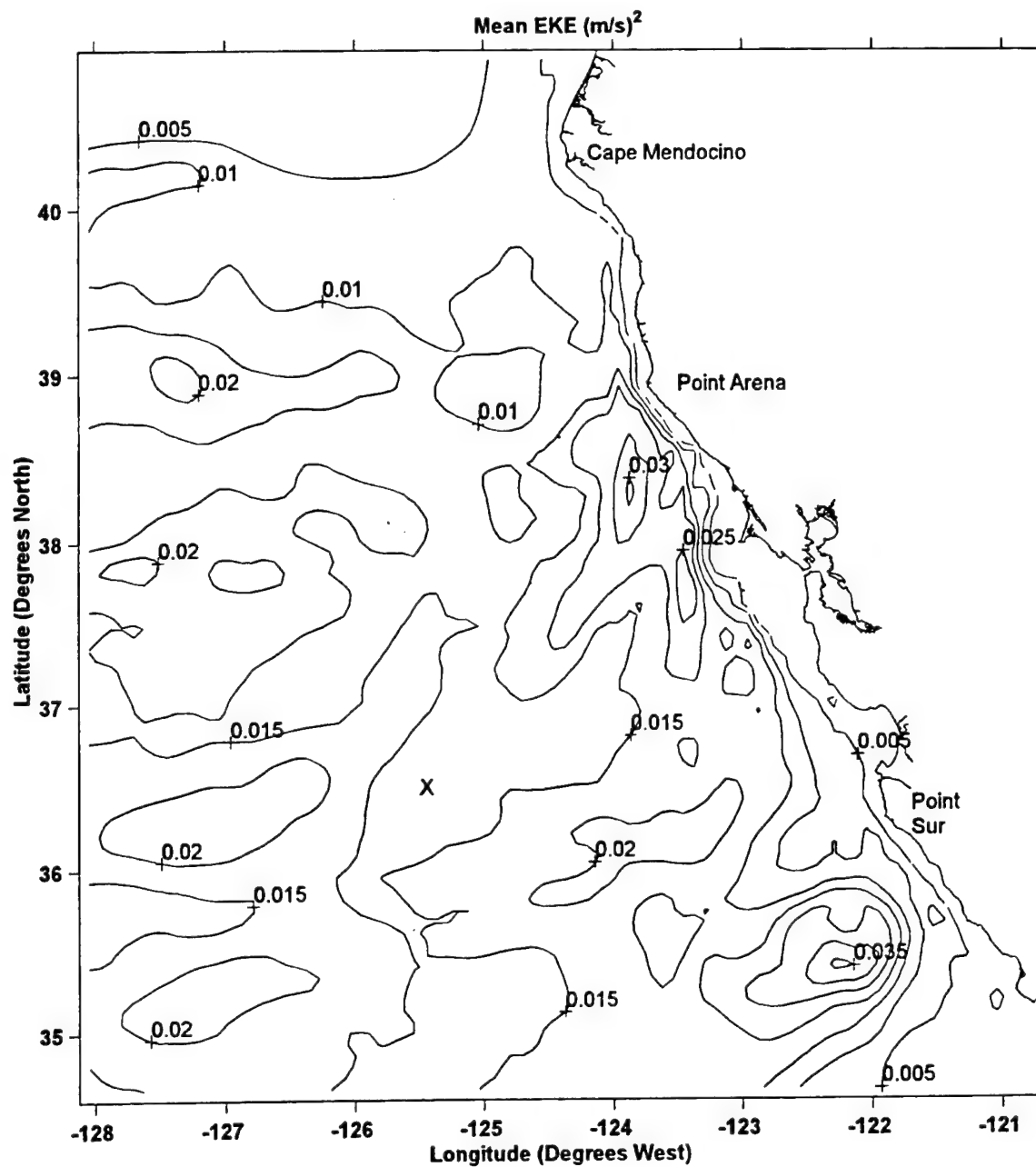
43

Figure 3.3 - Time mean Eddy Kinetic Energy in $(m/s)^2$. Contour interval is 0.005 $(m/s)^2$. The "X" at approx. 36.5°N, 126.5°W marks the location of the maximum value observed by Kelly *et al.*, 1998.

observations therefore do not include the coastal area east of 124°W where the model simulated EKE is largest.

The simulated EKE field in Figure 3.3 shows a general minimum near 125°W at most latitudes. West of about 125.5°W, and south of about 40°N the EKE increases westward, showing that energy is either being generated locally or is trapped/not efficiently dissipated at the western boundary. The normal expectation is that energy generated at or near the coast would propagate westward and either dissipate and/or be dispersed through a deeper column of water leaving lower energy levels at the western boundary for any given layer. It is also expected that EKE would only be generated at or near the coast as a result of coastal upwelling and wind driven eddy generating dynamics at the surface. To further investigate the seemingly abnormally high energy levels near the western boundary the EKE at two lower levels were examined. Figure 3.4 not only shows that higher energy levels exist west of about 124.5°W at the deep levels of 9 (392 m) and 14 (113 m), but energy levels are actually increasing toward the western boundary. This is not consistent with the normal expectation that energy levels should be decreasing westward. Thus, a working hypothesis at this stage is that the westward increase in EKE west of about 125°W at all levels is due to an artificial reflection of energy from an
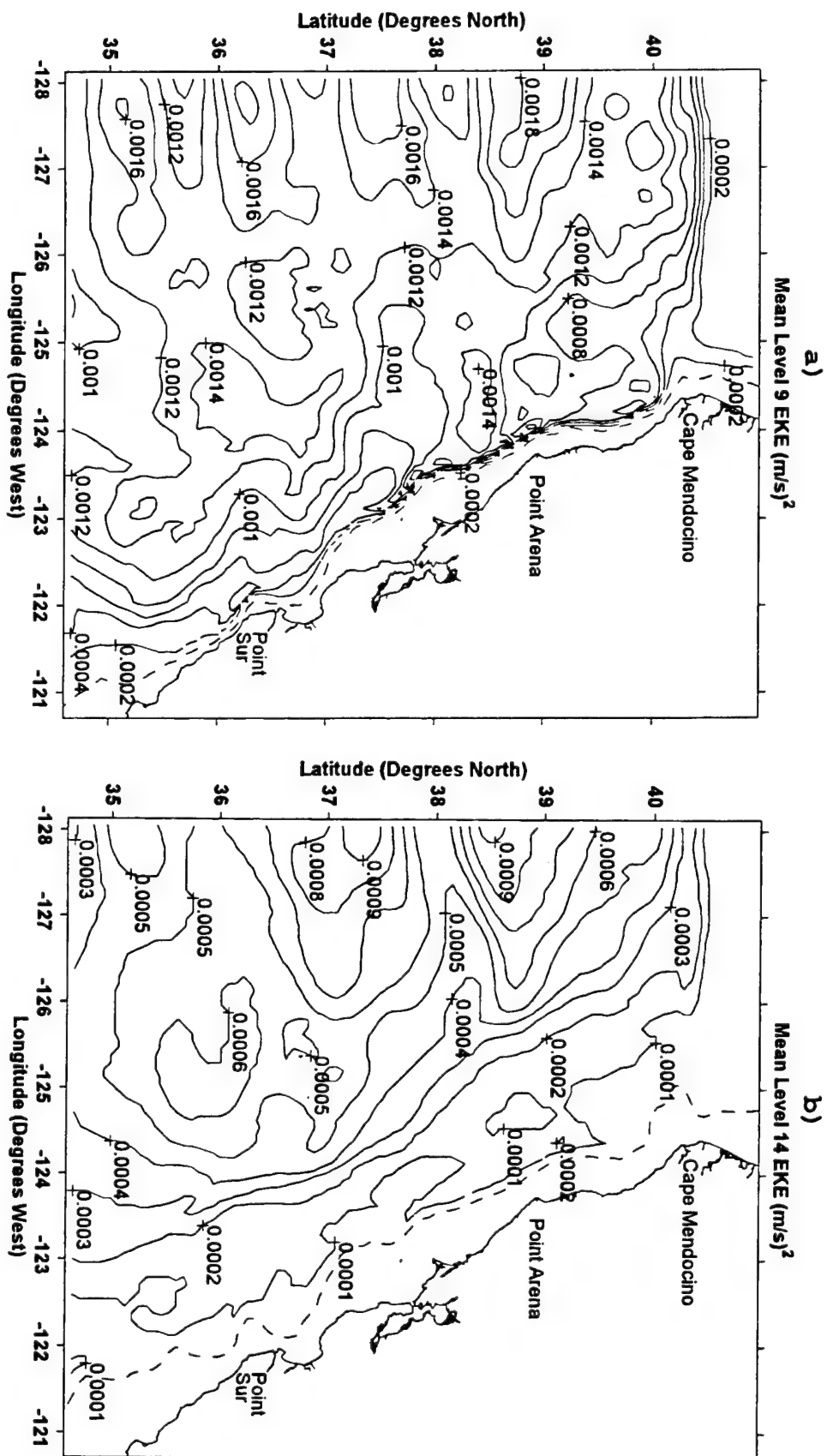
45

Figure 3.4 – a) Mean Eddy Kinetic Energy at level 9 (362 m). Contour interval is 0.0002 (m/s)². **b)** Mean EkE at level 14 (1141 m). Contour interval is 0.0001 (m/s)². The innermost dashed lines adjacent to the coast represent the topographic demarcation at that level.

46

incompletely "open" western boundary.

2.   Temporal Changes In Eddy Kinetic Energy

To avoid possible influences from the western boundary, the EKE fields were further analyzed in a coastline relative frame of reference.   This domain of analysis extends 3.75 degrees of longitude (about 330 km) westward from the coastline at each latitude. This region extends well into the deep water beyond the continental slope (Figure 2.0), but it excludes the region of artificial western boundary influence. Because the continental slope extends westward with increasing depth, the easternmost data point for lower levels (the coastline of those levels) also moves westward.   This means that the horizontal width of the domain at each successively lower level decreases slightly as the western edge of the domain is fixed (330 km west of the coastline at the surface).

Figure 3.5a shows the time evolution of the EKE at the surface (level 1 (10 m)), averaged over this coastline relative domain.   The time series shows a consistent pattern of peak seasonal energy levels occurring in the month of May/June.   The maximum observed value is 0.0241 (m/s)^2. Maximum values occur in late spring/early summer and appear to coincide with the annual cycle of headland winds (Figure 2.1a).   The minimum value of 0.0069 (m/s)^2 occurs in late fall/early winter and also appear to correspond to the annual
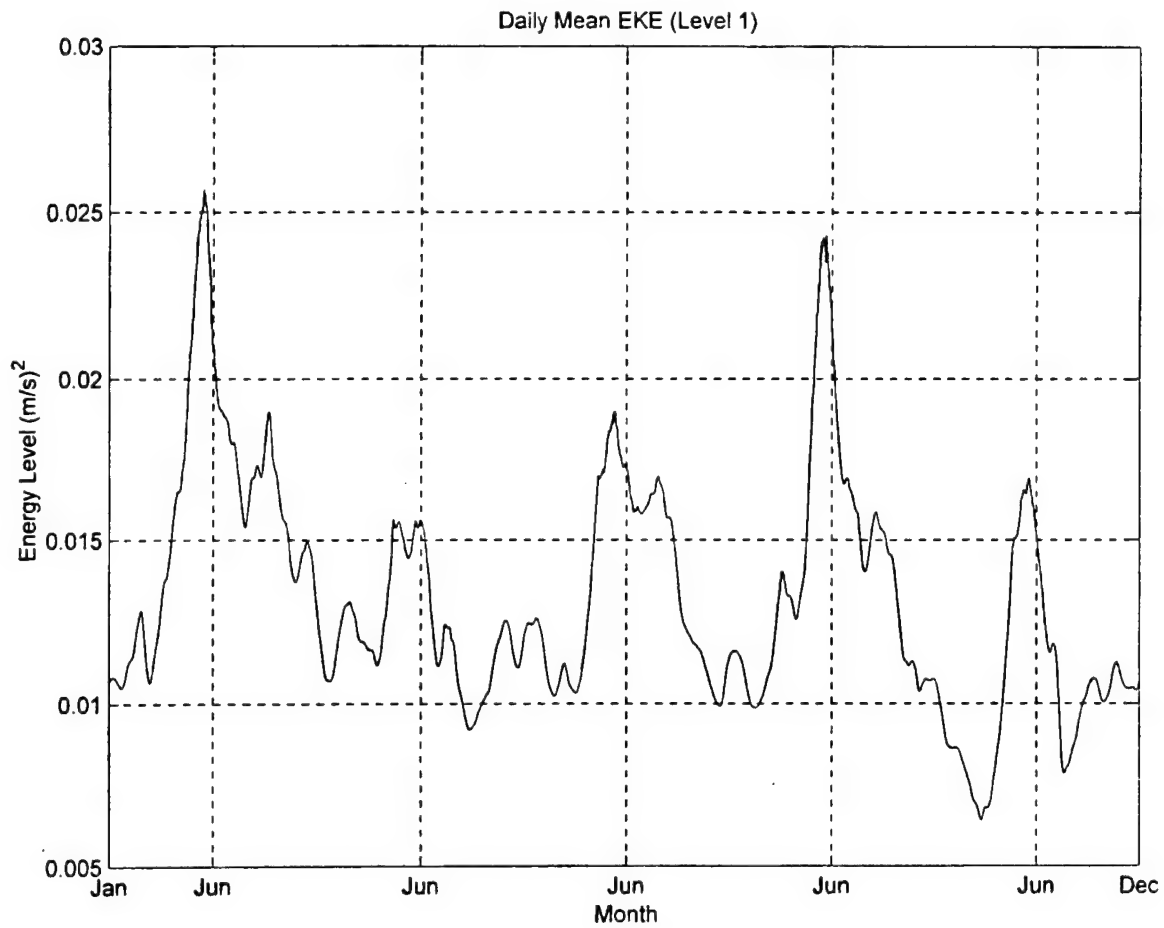
47

Figure 3.5a – Daily mean Eddy Kinetic Energy at the surface (level 1 (10 m)). Energy level is in $(m/s)^2$.

cycle of the headland winds. As noted in a previous section, the EKE time variability appears to be seasonally adjusted at about 0.0133 $(m/s)^2$ for an annual mean. These values correspond to eddy current speeds of about 8-16 cm/s with a mean of about 12 (cm/s). This compares with the two years of EKE from drifter data in Kelly et al. (1998) which shows maximum values of about 0.02 $(m/s)^2$ occurring in late summer/fall and minimum values of about 0.01 $(m/s)^2$ occurring in the early spring. As noted earlier however, the EKE values in Kelly et al. (1998) are averaged over a 700 x 900 km region entirely west of 124°W (i.e. well seaward of the slope) whereas the EKE values in Figure 3.5 are averaged over a region within 330 km of the coast. The simulated EKE reaches its maximum value earlier in the year (spring) than the observed EKE (summer/fall) because of the east-west difference in averaging domains (simulated verses observed) and because the EKE has a pronounced westward propagation as described in the next section.

Figure 3.5b shows the time evolution of the EKE below the main thermocline (level 9 (392 m)). As expected, the seasonal signal at the surface appears to be reflected in the lower level at reduced amplitude and time lagged. The peak energy level now appears to be in the late summer/early to mid fall.
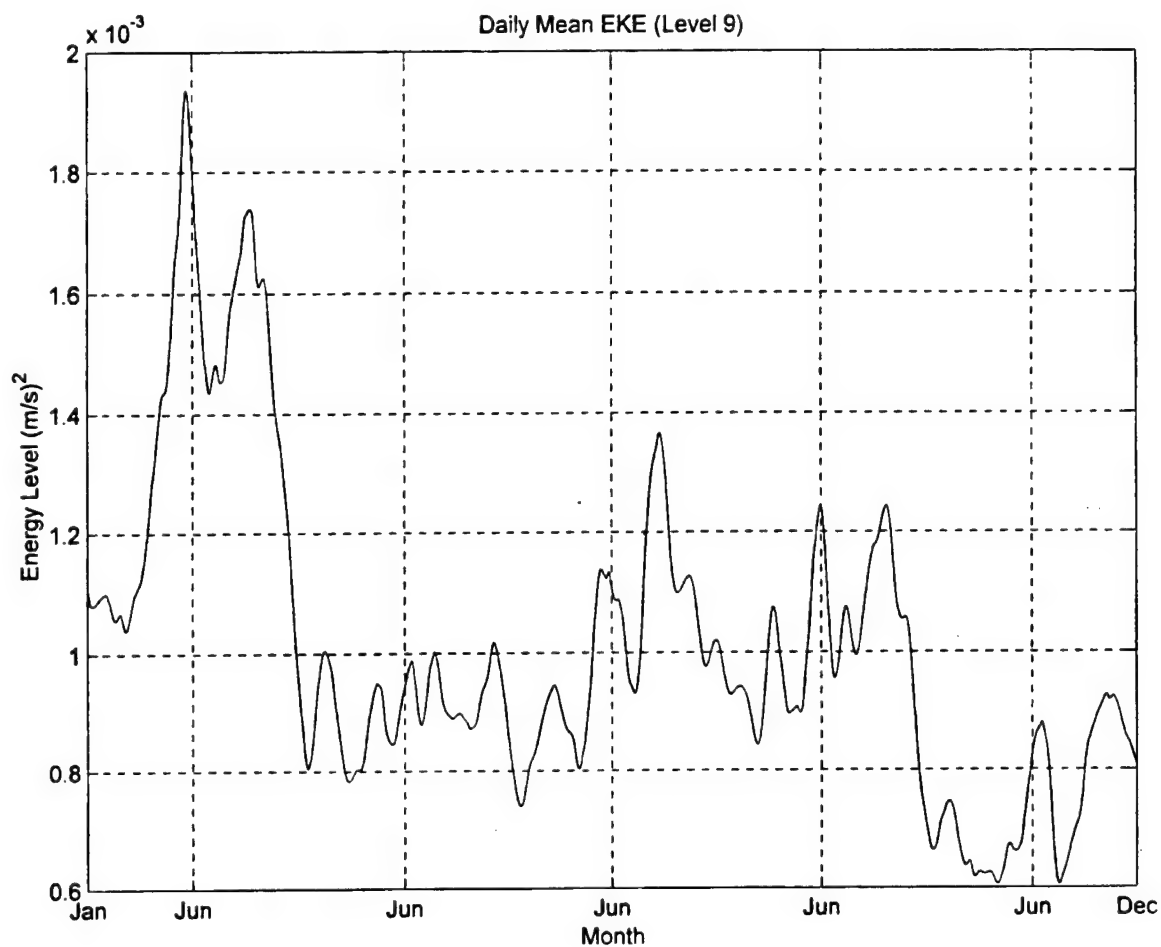
Figure 3.5b - Daily mean Eddy Kinetic Energy in the thermocline (level 9 (392 m)). Energy level is in $(m/s)^2$.

3.   Propagation of Eddy Kinetic Energy

One of the most robust features of the EKE analysis of Kelly *et al.* (1998) is the distinct westward propagation and decrease of EKE away from its source near the coast.   To examine this characteristic in the model simulation, Figure 3.6a shows a time distance (longitude) plot of the along-coast averaged EKE at the surface. As noted above, the analysis is performed over the coast relative domain.   The left edge of the plots in Figure 3.6 are 330 km from the coastline (at the surface) while the right edge of the plots are at the coastline appropriate for the given level.   The first evident feature is that high energy bands occur on a periodic basis, about every June, as expected. This EKE generation is clearly in connection with the spring/summer upwelling regime produced by the surface wind forcing.   A tendency for offshore propagation with time is also evident.   The peak EKE band occurs between about 35-185 km west of shore, with maximum values occurring between 50-150 km west of the coastline, consistent with the annual mean EKE field of Figure 3.3.   The westward propagation rate is estimated to be on the order of two (2) km per day or about 0.023 m/s. By comparison, Kelly *et al.* (1998) observed that peak EKE values at the surface also occurred in the June/July time frame near the coast and the westward propagation rate was estimated at 0.03 m/s,
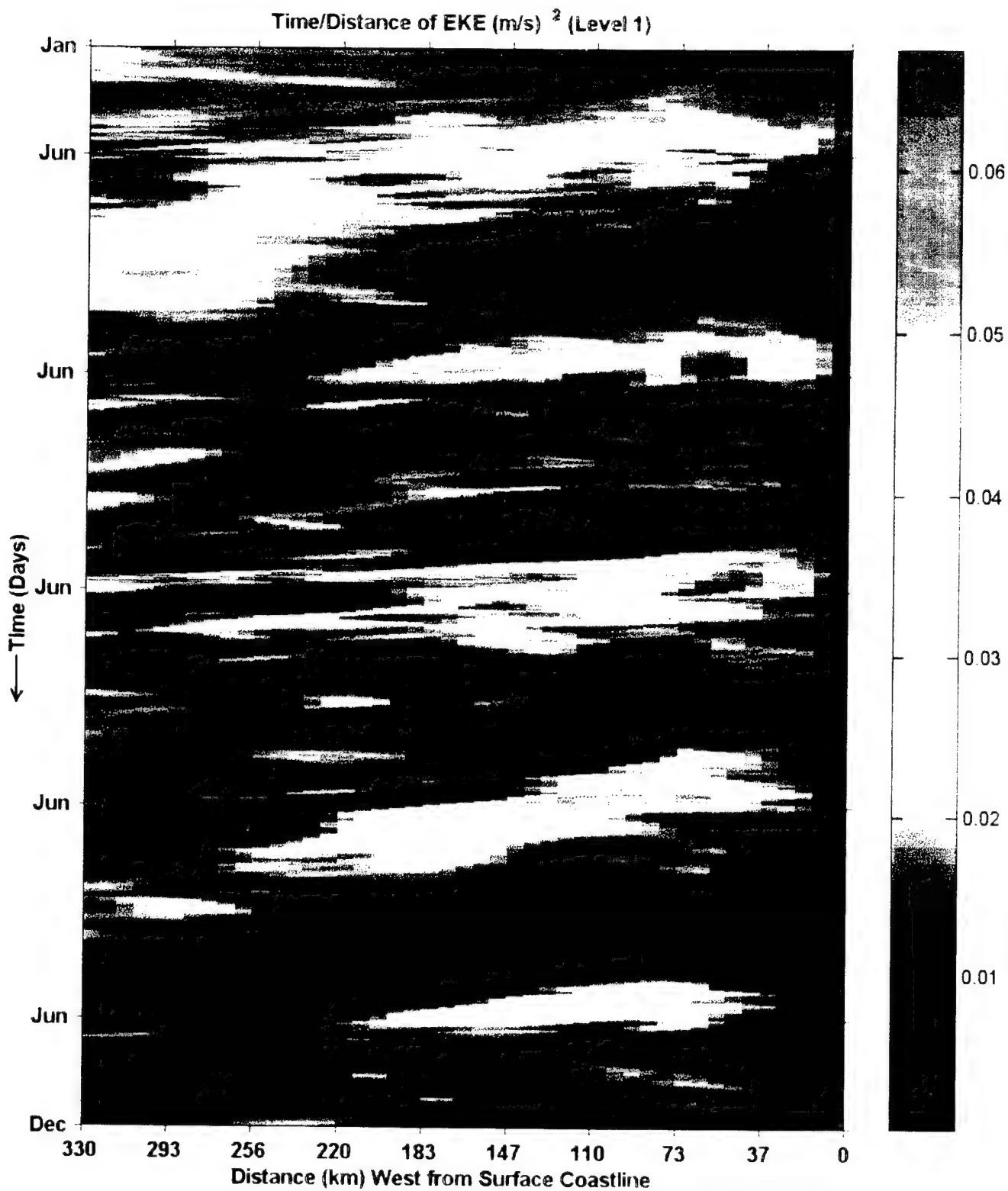
51

Figure 3.6a - Time and distance evolution of Eddy Kinetic Energy at the surface (level 1 (10 m)). EKE is plotted in days verses km from surface coastline. EKE is measured in

somewhat faster than observed in this study. These speeds of propagation are consistent with the speed of non-dispersive first mode Rossby waves at this latitude.

Time distance plots of EKE at levels 9 (392 m) and 14 (1139 m), shown in Figures 3.6(b,c), continue to show the westward propagation of EKE as expected. Most importantly the largest energy signals occur progressively farther offshore with depth, consistent with the energy moving out from the coast and penetrating downward with time. This vertical redistribution of EKE to the deep ocean west of its source near the coast partly explains the westward decrease of EKE at the surface that was documented in the California Current region by Kelly *et al.* (1998) and Strub and James (1998). The strong seasonal signal apparent at the surface becomes incoherent and gets blurred with depth, where the time interval between energetic events appears to be of the order of only 1-2 months.

Figure 3.6b - Time and distance evolution of Eddy Kinetic Energy at level 9 (392 m)). EKE is plotted in days verses km from surface coastline. EKE is measured in $(m/s)^2$.
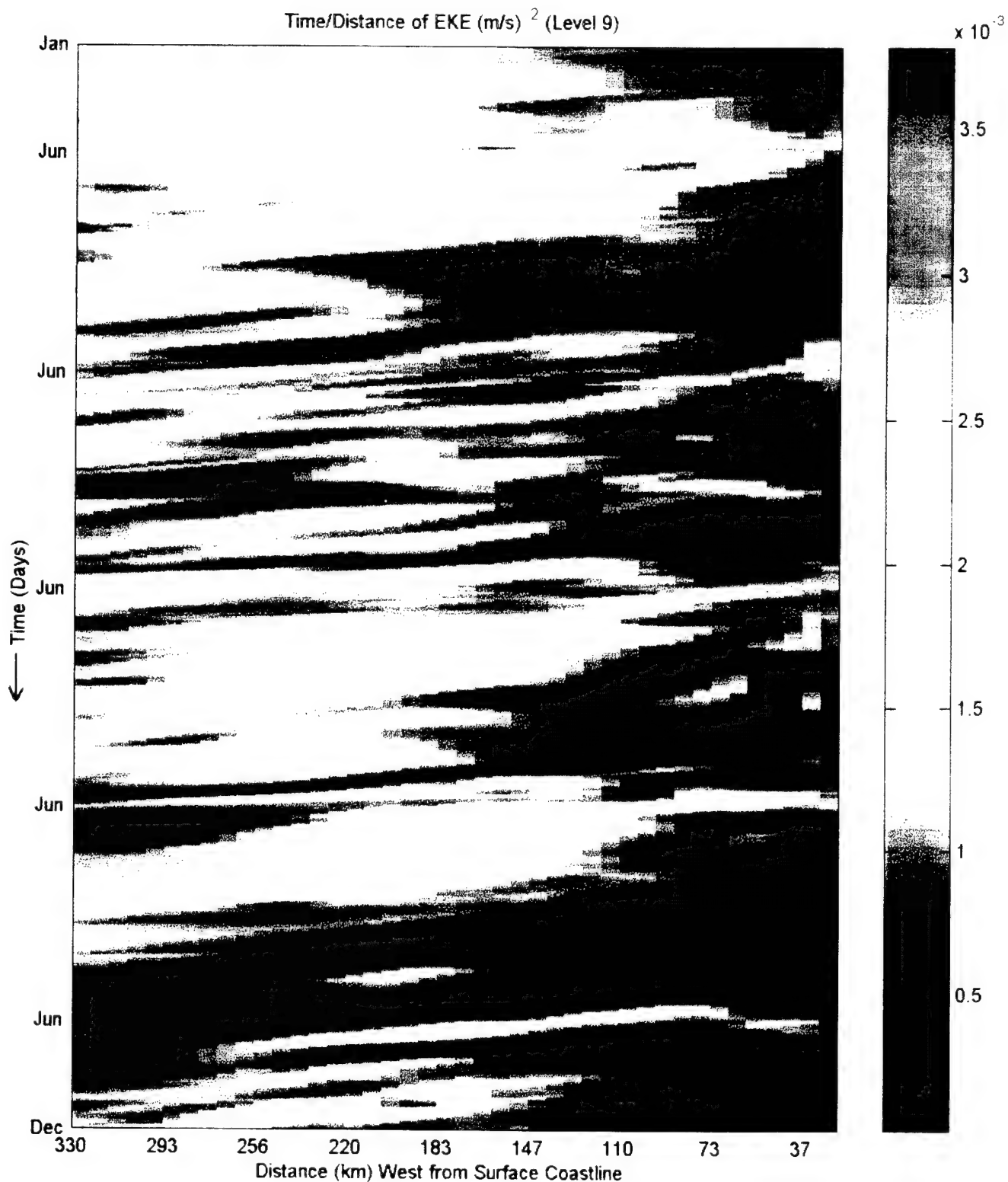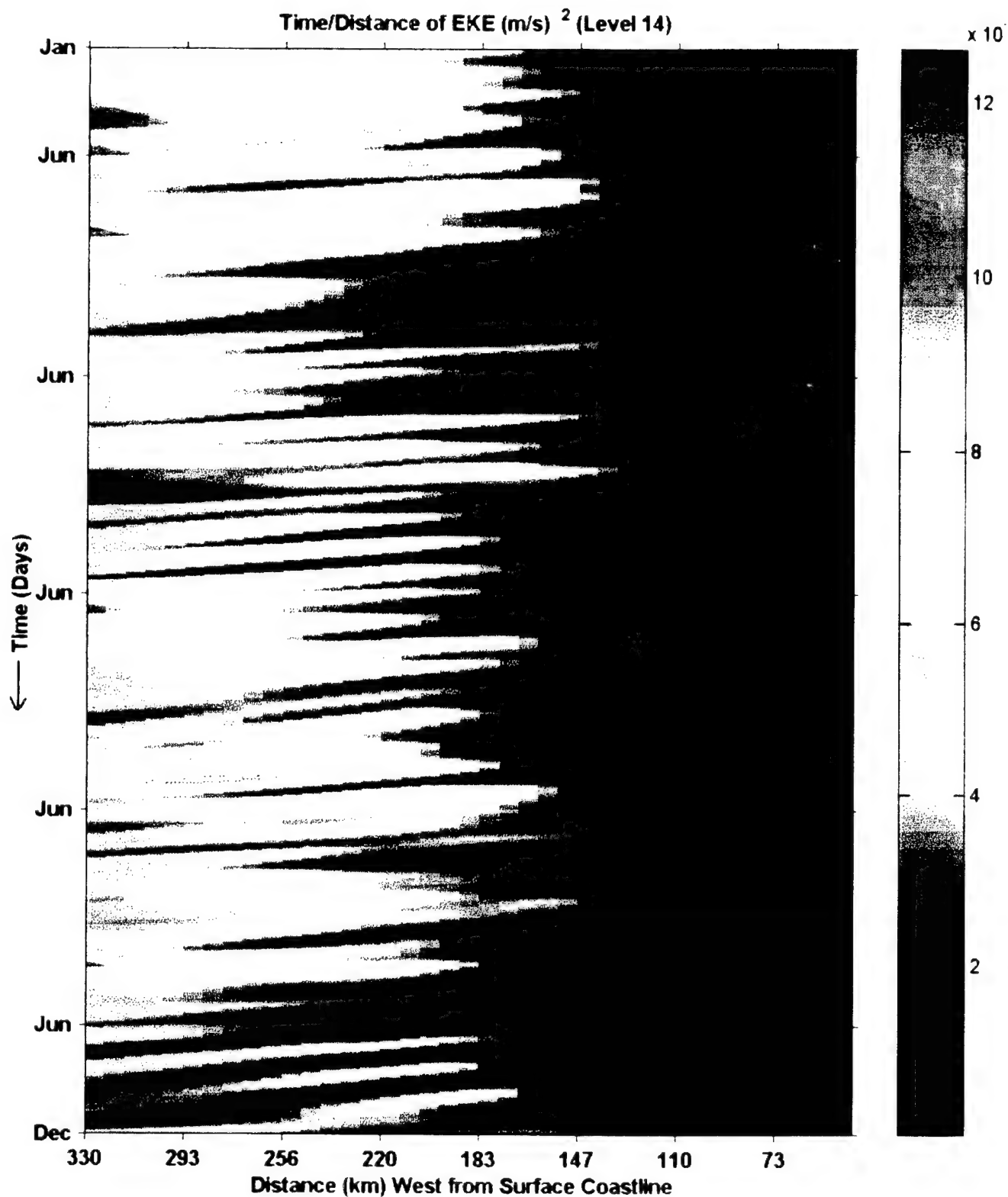
Figure 3.6c - Time and distance evolution of Eddy Kinetic Energy at level 14 (1139 m). EKE is plotted in days verses km from surface coastline. EKE is measured in $(m/s)^2$.

IV. SUMMARY, CONCLUSIONS AND RECOMMENDATIONS

An updated version of the DIECAST ocean model was used to conduct a numerical simulation study of mesoscale variability in the California coastal zone. Improvements to the model included an annual cycle of surface wind forcing, headland wind enhancements, surface buoyancy damping, and time phased barotropic and baroclinic across boundary jets. Specific model results were then compared to recent in-situ and remote sensing studies.

A. SUMMARY OF RESULTS

The observed mean dynamic sea surface height generally shows southwest geostrophic flow north of Point Arena and southeast flow south of Point Arena. Model simulated height values run generally parallel to the coast, but with a trough immediately south of Cape Mendocino, contrary to observations. The total height range over the entire model domain is 0.24 m, about 10% higher than observations. The strongest annual mean geostrophic currents are about three times stronger in the simulation than observed. There is also considerably more structure and along shore variability in the simulated mean dynamic height field than in the observed height field.

The seasonal sea surface height and sea surface temperature fields produced by the model show considerable

57

similarities in structure to observation however, the model shows stronger gradients in both the temperature and height fields throughout the four seasons than is observed. The southward coastal jet, always present in the model simulation, remains quasi-stationary and close to the coast. The jet pulses in strength, i.e. strengthens and weakens over the seasons vise relaxing and moving off shore during the non upwelling season and then reforming adjacent to the coast the next spring.

The simulated mean eddy kinetic energy field shows considerable structure and variability, with two main regions of eddy energy production adjacent to the coast, one just south of Point Arena and one south of Point Sur. Near shore observations of EKE are not available for comparison but an offshore study (Kelly *et al.*, 1998) showed a single maximum of eddy energy west of Monterey Bay, in between the two regions the model simulated eddy kinetic energy maxima. Eddy energy decreases between about 124°W and 126°W then re-intensifies west of 126°W to the western boundary. The investigation of this phenomena at lower levels revealed that there is likely to be western boundary influences contaminating the simulated data from the western boundary eastward to about 126°W.

Because of this, a coastline relative domain was developed to minimize the possible influence of the western

boundary on the analysis and interpretations.

The temporal changes in eddy kinetic energy averaged over the coastal region showed a definite strong seasonal cycle in phase with the coastal winds and in agreement with the analysis of Kelly et al. (1998). The simulated energy levels at the surface are somewhat higher than observations but the differences are not considered significant since the domains being compared are somewhat different. The simulated phase in amplitude appears to coincide with the surface wind forcing. The surface energy signal appears to be reflected at lower levels, weakening and lagging in time as expected.

The time-longitude evolution of eddy kinetic energy averaged along the coast shows a seasonal signal and westward propagation consistent with both temporal changes in eddy kinetic energy and westward propagation seen in observations. Our westward propagation rate is estimated to be somewhat slower than in observations, but the difference is not considered significant. The downward spreading of eddy energy is evident in the simulation with peak EKE levels occurring further and further offshore with depth, while the seasonal signal of EKE becomes indistinguishable at depth.

B. CONCLUSIONS AND RECOMMENDATIONS

Results indicate that the use of improved model physics can produce ocean variability generally consistent with

59

observations in the California coastal zone, but with important differences as well.

The result that the model produced a stronger gradient of mean dynamic sea surface height than observed may be a combination of several factors of model dynamics. As mentioned earlier, the structure and magnitude of the actual headland winds is still in question and under investigation. The fact that the headland winds were modeled to oscillate in place on a yearly cycle may be too simplified compared to observations that show "upwelling favorable events" occur on a periodic basis, lasting perhaps several days, rather than remaining constant and diminishing on a monthly basis. The result of the enhanced upwelling may be such that the colder temperatures along the coast produce lower dynamic sea surface heights thereby increasing both the horizontal pressure and temperature gradients. This in turn may be the cause of the stronger than observed geostrophic velocities simulated along the upwelling front.

To test the possibility that the headland winds are responsible for the stronger coastal currents (and SSH gradients) a control experiment should be conducted without the headland winds to see if the overall intensity of upwelling is reduced sufficiently to produce more realistic values and behavior of sea surface height and temperature

while maintaining the proper structure. To further enhance the simulation, the surface wind stress forcing with Hellerman and Rosenstein (1983) mean monthly climatological wind fields could be replaced with data from a high resolution atmospheric model that shows a more realistic spatial and temporal variability in the wind stress field. This would eliminate the need for an idealized headland wind enhancement if the atmospheric model can properly produce the headland wind structure, including its synoptic and seasonal variability.

The high levels of eddy kinetic energy west of about 126°W to the western boundary are most likely caused by artificial interactions with the western boundary. As stated earlier, this may be the result of an improper (incompletely open) boundary condition not allowing the free and efficient exchange of energy across the western boundary. The cycle of the barotropic and baroclinic conditions at the northern and southern boundaries are less problematic because eddy propagation is zonal (westward). Nevertheless, as seen in the reduced area/coastline relative domain, results can be interpreted devoid of the western boundary influence.

One solution to the western boundary problem would be to make an ever bigger domain to increase the size of the buffer zone and thereby lessen the effects of the western boundary influence. This however would require significantly increased

processing and data storage resources, not a very appealing option. One other solution would be to "nest" the DIECAST model into an ocean basin model, like that of Semtner and Chervin (1992) or a larger DIECAST domain, where fully interactive boundary conditions can be used. This would be the most appealing option and likely to yield the most satisfactory results.

In spite of the above shortcomings, the simulation showed a pronounced tendency for offshore and downward propagation of eddy kinetic energy with time, and the rate of westward propagation is consistent with observations. The downward spreading of EKE offshore in the simulation (Figure 3.6) offers a possible interpretation of the westward decrease of EKE at the surface found in the recent observational analyses by Kelly *et al.* (1998) and Strub and James (1998). It is hypothesized that coastal eddies develop via baroclinic instability in the upper ocean in the vicinity of the continental slope, and as the eddies develop and propagate westward they transfer EKE to the deep ocean in a process similar to the occlusion process in atmospheric cyclones. Further study is clearly needed to test such a hypothesis.

The conclusion of this study is that the model simulation utilizing advanced second order physics can produce results consistent with observations and can provide insight to

interpret such observations. The inclusion of these advanced dynamics provides a significant improvement in the "realism" of the simulation over that carried out by Akahoshi (1995), but there is considerable room for additional improvements especially with regard to wind forcing and the treatment of open boundaries.

LIST OF REFERENCES

Akahoshi, S.A., 1995: DIECAST Model Simulation of the California Coastal Zone. Masters Thesis, Naval Postgraduate School, Monterey CA, 99 pp.

Burk, S.D., and W.T. Thompson, 1989: A Vertically Nested Regional Numerical Weather Prediction Model with Second Order Closure Physics. *Monthly Weather Review,* 117:2305-2324.

Burk, S.D., and W.T. Thompson, 1996: The Summertime Low-Level Jet and Marine Boundary Layer Structure Along the California Coast. *Monthly Weather Review,* 124:4,668-686.

Clancy, R.M., P.M. Phoebus, and K.D. Pollack, 1990: An Operational Global-Scale Ocean Thermal Analysis System. *J. Atmos. Oceanic Technol.,* 7:233-254.

Dietrich, D.E., 1997: Application of a Modified Arakawa "a" Grid Ocean Model having Reduced Numerical Dispersion to the Gulf of Mexico Circulation. Dynamics of Atmospheres and Oceans, 27:201-217.

Dorman, C.E., D.P. Rogers, W. Nuss, W.T. Thompson, 1998 (in review): Adjustment of the Summer Marine Boundary Layer Around Pt. Sur, California. 49 pp, *Monthly Weather Review,* submitted.

Enriquez A.G., and C.A. Friehe, 1995: Effects of Wind Stress and Wind Stress Curl Variability on Coastal Upwelling. *J. Phys. Oceanogr.,* 25:7,1651-1671.

Hellerman, S., and M. Rosenstein, 1983: Normal Monthly Wind Stress over the World Ocean with Error Estimates. *J. Phys. Oceanogr.,* 13,1093-1104.

Hodur, R.M., 1987: Evaluation of a Regional Model with an Update Cycle. *Monthly Weather Review,* 115:2707-2718.

Kelly, K.A., R.C. Beardsley, R. Limeburner, K.H. Brink, J.D. Paduan, T.K. Chereskin, 1998: Variability of the Near-Surface Eddy Kinetic Energy in the California Current Based on Altimetric, Drifter, and Moored Current Data. *J. Geophys. Res.,* 103:6,13067-13083.

Kosro, P.M., A. Huyer, S.R. Ramp, R.L. Smith, F.P. Chavez, T.J. Cowles, M.R. Abbott, P.T. Strub, R.T. Barber, P. Jessen, L.F. Small, 1991: The Structure of the Transition Zone Between Coastal Waters and the Open Ocean off Northern California, Winter and Spring 1987. *J. Geophys. Res.,* 96:8,14707-14730.

Levitus, S., Climatological Atlas of the Worlds Oceans, 1982: *NOAA Prof. Paper 13,* U.S. Government Printing Office, Washington D.C., 173 pp.

McCreary, J.P., Y. Fukamachi, P.K. Kundu, 1991: A Numerical Investigation of Jets and Eddies Near an Eastern Ocean Boundary. *J. Geophys. Res.,* 96:2,2515-2534.

National Oceanic and Atmospheric Administration (NOAA), 1986: ETOP05 Digital Refief of the Surface of the Earth, *Data Announce. 86-MGG-07, Natl. Geophys. Data Cent., Washington, D.C.*

Rogers, D.P., C.E. Dorman, K.A. Edwards, I.M. Brooks, W.K. Melville, S.D. Burk, W.T. Thompson, T. Holt, L.M. Strom, M. Tjernstrom, B. Grisogono, J.M. Bane, W.A. Nuss, B.M. Morley, and A.J. Schanot, 1998: Highlights of Coastal Waves 1996. *Bull. Amer. Meteor. Soc.,* 79:7,1307-1326.

Semtner, A.J., and R.M. Chervin, 1992: Ocean General Circulation From a Global Eddy-Resolving Model. *J. Geophys. Res.,* 97:4,5493-5550.

Strub, P.T., and C. James, 1998 (in review): Altimeter-derived Variability of Surface Velocities in the California Current System: 2. Seasonal Circulation and Eddy Statistics. Deep-Sea Research (submitted).

INITIAL DISTRIBUTION LIST

No. Copies

1. Defense Technical Information Center 2
    8725 John J. Kingman Rd., STE 0944
    Ft. Belvoir, VA 22060-6218

2. Dudley Knox Library 2
    Naval Postgraduate School
    411 Dyer Rd.
    Monterey, CA 93943-5101

3. Professor C.H. Wash, Chairman 1
    Code MR/Wx
    Naval Postgraduate School
    589 Dyer Rd., Rm 254
    Monterey, CA 93943-5114

4. Dr. Robert L. Haney 3
    Code MR/Hy
    Naval Postgraduate School
    589 Dyer Rd., Rm 254
    Monterey, CA 93943-5114

5. Dr. Roger T. Williams 1
    Code MR/Wu
    Naval Postgraduate School
    589 Dyer Rd. Rm 254
    Monterey, CA 93943-5114

6. Dr. Manny D. Fiadeiro 1
    Office of Naval Research
    Navy Ocean Modeling and Prediction
    800 N. Quincy St.
    Arlington, VA 22217

7. LT Joseph R. Donato 2
    441 Salem End Rd.
    Framingham, MA 01702-5523

8. Dr. David Dietrich 1
    1421 Monte Largo Dr., N.E.
    Albuquerque, MN 87112

9.   Fabrice Ardhuin, LT/FR NAV 1
      Code MR
      Naval Postgraduate School
      589 Dyer Rd., Rm 254
      Monterey, CA 93943-5114

10.   Dr. Julie McClean 1
      Code OC/Mn
      Naval Postgraduate School
      833 Dyer Rd. Rm 328
      Monterey, CA 93943-5122

REPRODUCTION QUALITY NOTICE

This document is the best quality available. The copy furnished to DTIC contained pages that may have the following quality problems:

- Pages smaller or larger than normal.

- Pages with background color or light colored printing.

- Pages with small type or poor printing; and or

- Pages with continuous tone material or color photographs.

Due to various output media available these conditions may or may not cause poor legibility in the microfiche or hardcopy output you receive.

☑ If this block is checked, the copy furnished to DTIC contained pages with color printing, that when reproduced in Black and White, may change detail of the original copy.